1 **Author's Accepted Manuscript**

2 **Phytoplankton absorption predicts patterns in primary productivity in Australian**

3 **coastal shelf waters**

4

5 Charlotte M. Robinson, Nagur Cherukuru, Nick J. Hardman-Mountford, Jason D. Everett,

6 M. James McLaughlin, Kevin P. Davies, Virginie Van Dongen-Vogels, Peter J. Ralph,

7 Martina A. Doblin.

8

9 Appears in Estuarine, Coastal and Shelf Science, Volume 192, 5 June 2017

10 DOI: 10.1016/j.ecss.2017.04.012

11

# Phytoplankton absorption predicts patterns in primary productivity in Australian coastal shelf waters

Robinson, C.M.[a,b,c*], Cherukuru, N.[b], Hardman-Mountford, N.J.[d], Everett, J.D.[a,e,f], McLaughlin, M.J.[d], Davies, K.P.[g], Van Dongen-Vogels, V.[a], Ralph, P.J.[a], Doblin, M.A.[a]

a. Climate Change Cluster, University of Technology Sydney, PO Box 123 Broadway, NSW 2007, Australia
b. CSIRO Oceans and Atmosphere, Black Mountain, GPO Box 1666 Canberra, ACT 2602, Australia
c. Remote Sensing and Satellite Research Group, Department of Physics and Astronomy, Faculty of Science and Engineering, Building 301, Curtin University, Bentley Campus WA 6102, Australia
d. CSIRO Oceans & Atmosphere, Indian Ocean Marine Research Centre (IOMRC), M097 35 Stirling Highway, Crawley WA 6009, Australia
e. Evolution & Ecology Research Centre, School of Biological, Earth and Environmental Sciences, University of New South Wales, Kensington, NSW 2052, Australia
f. Sydney Institute of Marine Science, Building 22, Chowder Bay Road, Mosman NSW 2088, Australia
g. School of Geosciences, Faculty of Science, University of Sydney, NSW 2006, Australia

*Corresponding author. Remote Sensing and Satellite Research Group, Department of Physics and Astronomy, Faculty of Science and Engineering, Building 301, Curtin University, Bentley Campus WA 6102, Australia

*Email address*: charlotte.robinson@curtin.edu.au

**Keywords:** phytoplankton, inherent optical properties, quantum efficiency, carbon fixation, bio-optics

**Abstract**

The phytoplankton absorption coefficient ($a_{PHY}$) has been suggested as a suitable alternate first order predictor of net primary production (NPP). We compiled a dataset of surface bio-optical properties and phytoplankton NPP measurements in coastal waters around Australia to examine the utility of an *in-situ* absorption model to estimate NPP. The magnitude of surface NPP (0.20 to 19.3 mmol C $m^{-3}$ $d^{-1}$) across sites was largely driven by phytoplankton biomass, with higher rates being attributed to the microplankton (> 20 μm) size class. The phytoplankton absorption coefficient $a_{PHY}$ for PAR (photosynthetically active radiation; $\bar{a}_{PHY}$)) ranged from 0.003 to 0.073 $m^{-1}$, influenced by changes in phytoplankton community composition, physiology and environmental conditions. The $a_{PHY}$ coefficient also reflected changes in NPP and the absorption model-derived NPP could explain 73 % of the variability in measured surface NPP ($n$ = 41; RMSE = 2.49). The absorption model was applied to two contrasting coastal locations to examine NPP dynamics: a high chlorophyll-high variation (HCHV; Port Hacking National Reference Station) and moderate chlorophyll-low variation (MCLV; Yongala National Reference Station) location in eastern Australia using the GIOP-DC satellite $a_{PHY}$ product. Mean daily NPP rates between 2003 and 2015 were higher at the HCHV site (1.71 ± 0.03 mmol C $m^{-3}$ $d^{-1}$) with the annual maximum NPP occurring during the austral winter. In contrast, the MCLV site annual NPP peak occurred during the austral wet season and had lower mean daily NPP (1.43 ± 0.03 mmol C $m^{-3}$ $d^{-1}$) across the time-series. An absorption-based model to estimate NPP is a promising approach for exploring the spatio-temporal dynamics in phytoplankton NPP around the Australian continental shelf.

## 1. Introduction

Estimates of net primary productivity (NPP, photosynthetically produced organic carbon after respiratory losses) from marine phytoplankton provide information about the rate of carbon production for the marine food web (Cloern et al., 2014; Finkel, 2014; Westberry and Behrenfeld, 2014). Coastal shelf waters generate 29 % of the world's marine NPP within an area of just 11 % of the ocean's surface area (Finkel, 2014; Gazeau et al., 2004; Pauly and Christensen, 1995; Wollast, 1998). In the global context, average NPP in Australian coastal waters is low (Chavez et al., 2011; Cloern et al., 2014). However, our understanding of the temporal and spatial dynamics in NPP and its absolute magnitude is limited to a small number of studies involving traditional measurements made on board ships and in the laboratory (Everett and Doblin, 2015; Furnas and Carpenter, 2016 and references therein).

Satellites provide the opportunity to fill the vast temporal and spatial gaps in conventional measurements of phytoplankton NPP in Australian waters due to their near synoptic capture of ocean colour data (Hayes et al., 2005). However, algorithms are required to transform maps of ocean colour, the result of the absorption and scattering of light by water, phytoplankton and non-phytoplankton material, to a description of phytoplankton physiology (Barnes et al., 2014; Bouman et al., 2000) and an estimate of NPP in ocean ecosystems (Sathyendranath et al., 2009).

Empirical relationships or mechanistic models are used to link phytoplankton biological rates (such as growth rate and NPP) and photosynthetic parameters (carbon-to-chlorophyll-*a* ratio) with "more-easily" measured satellite products such as sea-surface temperature, irradiance or chlorophyll-*a* (via the assimilation number). These physical and biological proxies have proven to be highly variable in their efficacy for coastal waters (Everett and Doblin, 2015;

90 Mélin and Vantrepotte, 2015). This is largely due to the multivariate nature of environmental
91 and seasonal influences on phytoplankton physiology, that cannot always be summarised to a
92 constant value needed for empirical relationships (Behrenfeld et al., 2016). In addition, the
93 satellite retrieval of the commonly used biological parameter, chlorophyll-*a* (Chl-*a*), using
94 model inversion of satellite remote sensing reflectance ($R_{rs}$) is highly unreliable in coastal
95 waters (Tilstone et al., 2011). The inversion method is complicated due to the interference of
96 other optically active substances (suspended organic and inorganic matter, and coloured
97 dissolved organic matter) in the water-leaving reflectance (Aurin and Dierssen, 2012;
98 Odermatt et al., 2012) and variable atmospheric aerosols contributing to the top of the
99 atmosphere reflectance (Wang et al., 2007). Uncertainties with respect to chlorophyll-*a*
100 retrievals in coastal waters globally are a significant problem where the concentration of
101 optically active constituents, and hence inherent optical properties (IOPs) and specific
102 inherent optical properties (SIOPs; normalised to constituent concentration), are highly
103 variable, both temporally and spatially (Brando et al., 2012; Cherukuru et al., 2014; Qin et
104 al., 2007). In contrast, the phytoplankton absorption coefficient ($a_{PHY}$) can be more reliably
105 inverted from $R_{rs}$ using deconvolutions of total absorption ($a_{TOT}$) using semi-analytical
106 algorithms (Barker et al., 2007; Moore et al., 2009; Sauer et al., 2012). The Generalised IOP
107 model is one such algorithm which allows a high percentage (> 80 %) of valid retrievals of
108 $a_{PHY}$ in waters of all trophic levels and across all seasons (Werdell et al., 2013).
109
110 Replacement of the chlorophyll-*a* parameter with the phytoplankton absorption coefficient
111 ($a_{PHY}$) has been proposed as a viable alternative for estimating NPP in oceanic and coastal
112 waters (Barker et al., 2007; Barnes et al., 2014; Marra et al., 2007; Silsbe et al., 2016). This is
113 because the concentration of pigments within a cell changes in predictable ways with the
114 composition and abundance of phytoplankton and environmental conditions (light,

115 temperature, nutrients etc; Bouman et al., 2000; Marra et al., 2007; Aiken et al., 2008).
116 Furthermore, variation in the $a_{PHY}$ coefficient at different wavelengths (e.g. 440 nm vs 676
117 nm) or chlorophyll-specific phytoplankton absorption coefficient ($a^*_{PHY}(\lambda)$) are due to
118 changes in the physiology or composition of the phytoplankton community. Such changes
119 include taxonomic or pigment composition, cell size, pigment packaging or intracellular
120 pigment concentration (Aiken et al., 2008; Bouman et al., 2000; Bricaud et al., 2004).
121 Although phytoplankton absorption is a relatively inexpensive and simple parameter to
122 measure in marine sampling programs (Sathyendranath et al., 2009), there has been limited
123 application of this approach because of the lack of absorption data coupled with primary
124 productivity measurements (Barnes et al., 2014; Everett and Doblin, 2015; Marra et al.,
125 2007).
126
127 Absorption based models of primary productivity use the phytoplankton absorption
128 coefficient ($a_{PHY}(\lambda)$) as a first order predictor of NPP or as a light capture term to quantify the
129 absorption of photosynthetically active radiation (400-700 nm; PAR or *E*) which is then
130 utilised to fix inorganic carbon. The maximum efficiency of photon capture to carbon
131 conversion ($\phi_m$) varies with nutrient concentration and PAR (sometimes parameterised as
132 $\phi_E$; Kiefer and Mitchell, 1983). Generally, the absorption coefficient is measured directly
133 using an *in-situ* absorption meter, in the laboratory using a filter pad technique (Lee et al.,
134 1996; Oubelkheir et al., 2006; Tassan and Ferrari, 1995) or indirectly via inversion of in-
135 water and/or above-water radiance (Qin et al., 2007). The parameters describing the
136 partitioning and utilisation of light by the photosynthetic apparatus for photochemistry and
137 carbon fixation (e.g. $\phi_m$ and $\phi_E$) are often estimated from laboratory based studies with algal
138 monocultures (Marra et al., 2007, 2003). Despite the limited data from mixed natural
139 assemblages, absorption-based NPP models have reliably estimated NPP with low error,

using *in-situ* data in the Equatorial Pacific, Southern Ocean, Western English Channel, California coast, North Atlantic, and North Pacific (Barnes et al., 2014; Ma et al., 2014; Marra et al., 2007). Absorption-based models have also been applied to satellite inverted $a_{PHY}$ coefficient to study the dynamics of NPP in the Southern Ocean and global eastern boundary upwelling regions (Hirata et al., 2009; Shang et al., 2010) and provide global estimates of annual NPP (Ma et al., 2014)

To assess the utility of an absorption-based approach to estimate surface NPP in Australian coastal waters, this study compiled bio-optical and NPP data from tropical to temperate Australian locations. Using this unique dataset, we tested the hypothesis that light absorption by phytoplankton is a strong first-order predictor of surface phytoplankton NPP. The absorption-based model was then used to examine NPP dynamics in two contrasting regions on the East Australian coast – one in an area with low chlorophyll-*a* variation and another with relatively high chlorophyll-*a* variation (Jones et al., 2015).

## 2. Methods

### *2.1 Sampling sites*

Coastal waters around Australia were sampled during four oceanographic research voyages (V1-V4) and at a coastal time-series station (PHNRS) between 2010 and 2014. Sampling locations included the north-west Kimberley region (V1), eastern Australia (V2), northern Australia (V3), the Great Barrier Reef inner-reef (GBR; V4) and in south-eastern Australia at the Port Hacking National Reference Station (PHNRS; see Figure 1 and Table 1 for station locations). Water was collected at depths of up to 5 m (within the first optical depth) for surface measures of NPP, physico-chemical, biogeochemical, and bio-optical parameters (Table 1).

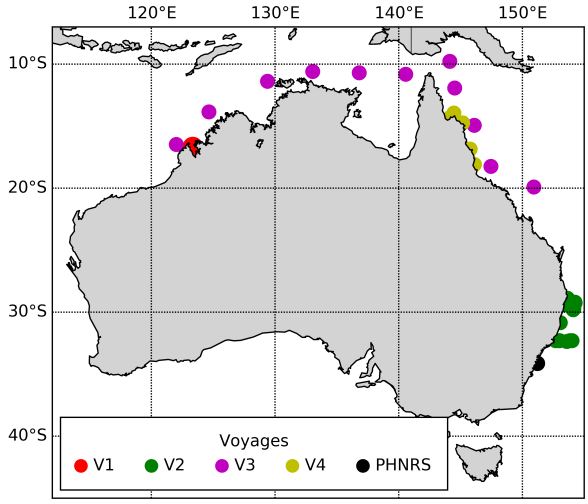


Figure 1. Locations of the stations sampled for *in-situ* parameters during each field campaign: SS2010_v03 (V1), SS2010_v09 (V2), SS2013_t03 (V3), eReefs (V4) and Port Hacking National Reference Station (PHNRS).

*2.2 In-situ sampling*

2.2.1 Net Primary Productivity

Samples (0.5-4.0 L) of surface seawater were incubated at *in-situ* temperature and light to estimate surface NPP. Stations sampled during V2, V3 and PHNRS were incubated for 24 h and stations sampled during V1 and V4 were incubated during the light period (1–6 h; Table 1). Water was dispensed into 0.5 – 4.0 L polycarbonate bottles and inoculated with 100 µmol $L^{-1}$ $NaH^{13}CO_3$ (V3 and V4) to achieve <5 % enrichment (Burford et al., 2011) or $NaH^{14}CO_3$ (V1, V2 and PHNRS) to achieve 20 µCi activity (Knap et al., 1996). After incubation, samples were filtered onto 25 mm glass fibre filters (Whatman GF/F 0.7 µm pore size; pre-combusted for $^{13}C$ assays).

Carbon uptake in all $NaH^{14}CO_3$ assays was measured using a liquid scintillation counter (Perkin Elmer, Massachusetts, USA). Total $NaH^{13}CO_3$ incorporation was analysed as per particulate organic carbon (see section 2.2.4 below). Carbon fixation rates were calculated according to the procedure of Hama et al. (1983) for $^{13}C$ and Knap et al. (1996) for $^{14}C$. NPP

185 was computed as a daily rate i.e. mmol C $m^{-3}$ $d^{-1}$ (Table 1). During V1, carbon fixation was
186 measured in 1 h *P* vs *I* assays using the "small bottle" method (Lewis and Smith, 1983). The
187 carbon fixation data from this assay was modelled using the equation of Platt et al. (1980) to
188 derive the photosynthetic parameters $P_m^B$, $\alpha^B$, $E_K$ and $\beta^B$. The chlorophyll-*a* (Chl-*a*) specific
189 maximum rate of photosynthesis ($P_m^B$) was then used to calculate daily NPP as per equation
190 (1) of Robinson et al. (2009) with a loss factor applied to account for daily respiration,
191 estimated at 30 % of carbon fixed (Steeman Nielsen and Hansen, 1958). Phytoplankton
192 respire at the same rate during the diel cycle (Grande et al., 1989; Langdon, 1993) and night-
193 time respiration has been reported to be between 25-40 % of daytime measured NPP (Bender
194 et al., 1999; Marra and Barber, 2004; Steeman Nielsen and Hansen, 1958). Daily NPP for
195 samples collected during V4 (4-6 h) was calculated using the day-length and corrected for
196 daily respiration as above. For samples incubated for 24 h during V2 and V3 it was assumed
197 that respiratory losses are accounted for in the final 24 h measurement of carbon assimilation
198 (Marra, 2009). It is recognised that there are differences in estimating carbon uptake using
199 $^{13}C$ vs $^{14}C$ methods; $^{14}C$ is a more sensitive technique where sample volume is limited,
200 however safety restrictions prevented the use of $^{14}C$ during some voyages. Nevertheless, $^{14}C$
201 and $^{13}C$ methods present the most consistent estimates of *in-situ* primary productivity when
202 compared with alternate techniques such as oxygen evolution and chlorophyll-*a* fluorescence
203 (Mousseau et al., 1995; Regaudie-de-gioux et al., 2014).
204
205 *2.2.2 Bio-optical parameters*
206 Samples to estimate particulate absorption ($a_{PART}$; $m^{-1}$) by phytoplankton pigments ($a_{PHY}$) and
207 non-algal detritus (NAP; $a_{NAP}$) were obtained by filtering seawater onto 25 mm GF/F filters
208 (Whatman GF/F, pore size 0.7 μm) for filter-pad measurements as per Tassan and Ferrari
209 (1995) and Mitchell et al. (2002). Samples collected from V3 and PHNRS were analysed

using a fibre optic UV/VIS spectrometer (Ocean Optics, Florida, USA) as in Robinson et al. (2014). Samples collected from V1, V2 and V4 were measured using a dual beam scanning spectrophotometer equipped with an integrating sphere (GBC 916 UV/VIS; Oubelkheir et al., 2014). Absorption (a(λ)) at wavelengths between 400 and 700 nm ($m^{-1}$) was calculated using equation (14) of Tassan and Ferrari (1995).

Water samples for coloured dissolved organic matter (CDOM) analysis were filtered through a 0.2 μm filter (Whatman ANODISC) and the final filtrate preserved for later analysis of absorbance as described in Cherukuru et al. (2014). Samples were analysed using a UV/VIS spectrophotometer; on a GBC916 UV/VIS (GBC Scientific equipment, Australia) for V1, V2 and V4 and on a Lambda 950 (Perkin Elmer, USA) for V3 and PHNRS.

Mean $a_{PHY}$, $a_{NAP}$ and absorption due to CDOM ($a_{CDOM}$) coefficients at 440 and 676 nm were calculated for two 8 nm bands, 437-444 nm and 673-680 nm, to avoid introducing small errors from the filter-pad technique into the data analysis (Barnes et al., 2014). For simplicity, the spectrally integrated coefficients for PAR e.g. $\bar{a}_{PHY} = \int_{400}^{700} a_{PHY} d\lambda / \int_{400}^{700} d\lambda = \int_{400}^{700} a_{PHY} d\lambda / 300$ are represented by $\bar{a}_{PHY}$, $\bar{a}_{NAP}$ and $\bar{a}_{CDOM}$, where the constant 300 accounts for a spectral range over 400 to 700 nm. The total absorption coefficient for PAR ($\bar{a}_{TOT}$) is the sum of $\bar{a}_{PHY}$, $\bar{a}_{NAP}$ and $\bar{a}_{CDOM}$. The spectral slopes of CDOM ($S_{CDOM}$) and NAP ($S_{NAP}$) were determined by applying an exponential model to fit $a_{CDOM}$ and $a_{NAP}$ between 400 and 700 nm (Babin et al., 2003).

232 *2.2.3 Water column profiles*

233 Alongside surface NPP incubations, vertical profiles of temperature, salinity and Chl-*a*
234 fluorescence were collected with a CTD (SeaBird SBE19+, Seattle, WA, USA). The mixed
235 layer depth (MLD) was defined from density profiles ($\sigma$; kg $m^{-3}$) as the depth where $\sigma=\sigma_{10m} \pm$
236 0.03 (de Boyer Montégut et al., 2004).

237

238 Measures of downwelled irradiance ($E_d$(PAR); µmol photons $m^{-2}$ $s^{-1}$)) were collected using a
239 2π upwards looking quantum cosine irradiance sensor (PAR, 400-700 nm; Biospherical
240 Instruments QCP=2300) during voyages V1 and V2, and hyperspectral spectroradiometers
241 during V3 and PHNRS (Ramses Trios, Rastede, Germany) and V4 (Satlantic,
242 http://satlantic.com/profiler). Hyperspectral measurements were trapezoidally integrated
243 between 400 and 700 nm to yield $E_d$(PAR). The diffuse attenuation coefficient $K_d$ ($m^{-1}$) for
244 PAR ($K_d$(PAR); i.e. integrated between 400-700 nm) was calculated by linear regression of
245 the natural logarithm of irradiances versus depth (equation 1.53, Kirk, 2011).

246

247 *2.2.4 Biogeochemical properties*

248 Surface water was sampled for macronutrient analyses (nitrate $NO_3$, silicate Si, phosphate
249 $PO_4$ and ammonia $NH_4^+$; µmol $L^{-1}$) for V1-3 and PHNRS. Hydrochemical analyses to
250 determine nutrient concentrations for V1-3 were carried out by CSIRO Marine and
251 Atmospheric Research (CMAR) according to Cowley et al. (1999). Seawater was preserved
252 with mercuric chloride and analysed for DIC as per Cowley et al. (1999) and Knap et al.
253 (1996).

254

255 Water samples (0.5-2.2 L) for particulate organic carbon (POC; for natural $^{13}C$ abundance),
256 and phytoplankton pigment concentration were filtered onto 25 mm GF/F filters (Whatman

GF/F 0.7 μm pore size; pre-combusted for POC) under low vacuum (<50 mg Hg) and stored at -80 °C. POC filters were dried at 60 °C for 24 h, and isotopic composition and total particulate carbon (and nitrogen) concentrations were determined using an elemental analyser (Thermo Finnigan MAT Conflo IV) coupled to an isotope ratio mass spectrometer (Thermo Finnigan Delta XP; University of Hawaii, USA).

Pigment concentrations were estimated using high performance liquid chromatography (HPLC) following the methods of Van Huelkelem et al. (2001). As a measure of phytoplankton light harvesting capacity, diagnostic pigment sums (Barlow et al., 2004) were applied to pigment concentrations to determine the proportion of photoprotective carotenoids in the total pigment pool (PPC/TP; alloxanthin, β-carotene, diatoxanthin, lutein, zeaxanthin). The pigment data were also partitioned to identify the contribution by pico-, nano- and microplankton size classes to the total phytoplankton community biomass using the diagnostic pigment criteria in Vidussi et al. (2001) and Uitz et al. (2006). The diagnostic pigment analyses were corrected according to Hirata et al. (2008), Brewin et al. (2010) and Devred et al. (2011) for the attribution of chlorophyll-*b*, 19'-hexanoloxyfucoanthin and fucoxanthin to the three size classes, as well as assigning samples to the picoplankton class where the total chlorophyll-*a* concentration was < 0.25 mg $m^{-3}$. The dominant size class of each sample was established based on whether a size class (pico-, nano- or microplankton) had a diagnostic pigment to chlorophyll-*a* ratio of greater than 0.45 as per Hirata et al. (2008). The ratio threshold was set at 0.45 rather than 0.5 to minimise the number of samples diagnosed as "mixed", that is, where no size class ratio is > 0.5.

*2.4 Absorption model development*

*In-situ* surface daily net primary productivity (mmol C $m^{-3}$ $d^{-1}$) was computed using four common forms of an absorption-based model: including application of a proportional factor to derive the photosynthetic rate *(NPP1*; Marra et al., 2007; Hirata et al., 2008), a mechanistic model with a fixed quantum efficiency for the conversion of photons to carbon (*NPP2*; Lee et al., 1996; Shang et al., 2010), and two size-class based models using size-based proportionality factors (*NPP3*; Hirata et al., 2008); and quantum efficiencies that were parameterised from the compiled data set (*NPP4*; Barnes et al., 2014).

$$NPP1 = \bar{a}_{PHY} \times p \quad (1)$$

$$NPP2 = \bar{E} \times \bar{a}_{PHY} \times \phi_m \times \phi_E \times 1000 \quad (2)$$

$$NPP3 = \bar{a}_{PHY} \times p_s \quad (3)$$

$$NPP4 = \bar{E} \times \bar{a}_{PHY} \times \phi \times 1000 \quad (4)$$

Where $\bar{a}_{PHY}$ is the phytoplankton absorption coefficient for PAR ($m^{-1}$), $p$ is the proportionality factor or slope between $\bar{a}_{PHY}$ and measured NPP (estimated as 304 from the compiled *in-situ* data ($n$ = 40) as compared to $p$ = 510 for Marra (2007)), and $\bar{E}$ is the daily incident PAR (integrated between 400-700 nm; mol photons $m^{-2}$ $d^{-1}$) at the depth of sampling. The daily incident PAR ($\bar{E}$) was derived from the daily MODIS Aqua 1 km Level 2 PAR product obtained from the Australian Integrated Marine Observing System (IMOS) for the day of *in-situ* sampling (DOS) or the mean of ± 4 days from the DOS. The irradiance ($E$) was normalised to the total absorption i.e. $\bar{E} \times (\bar{a}_{PHY} / \bar{a}_{TOT})$ to account for the fraction of light that is available for phytoplankton photosynthesis and not absorbed by other dissolved or particulate constituents of seawater (equivalent to *APAR*; Frouin and Kampel, 2014; Morel, 1991). Daily PAR at the depth of sampling was computed for a 3 x 3 pixel region

encompassing each station at its centre point using the *in-situ* measured attenuation coefficient for PAR, $K_d$(PAR) after correction for air-water transfer (Eqn 2.16, Kirk, 2011).

The parameter $\phi_m$ is the maximum quantum efficiency of photosynthesis and is fixed at 0.06 mol C mol photons$^{-1}$ (global average from Marra et al., 2003). The parameter $\phi_E$ describes the dependency of the quantum efficiency $\phi$ on $E$ (Kiefer and Mitchell, 1983; Shang et al., 2010) and can be expanded to:

$$\phi_E = (K_\phi \exp(-v \times E)/(K_\phi + E) \qquad (5)$$

Where $K_\phi$ is the irradiance at which the quantum efficiency is equal to $\phi_m/2$ (set at 10 mol photons m$^{-2}$ d$^{-1}$ as per Kiefer and Mitchell (1983)) and $v$ is a photoinhibition factor (0.01 mol photons m$^{-2}$ d$^{-1}$). In *NPP3* and *NPP4*, the proportionality factor ($p_s$) and quantum efficiency ($\phi$) respectively, are selected based on the dominant size class (micro-, nano-, pico-plankton) present in the sample determined using phytoplankton pigments (see details above section *2.2.4*). The proportionality factor for micro-, nano- and pico-plankton was quantified from the compiled *in-situ* data. The quotient of NPP and $\bar{a}_{PHY}$ was calculated for each sample within each size-class and the mean quotient (proportionality factor) was computed for each size class to represent micro-, nano- and pico-plankton (see Supplementary Table 1 for values). The quantum efficiency ($\phi$) for micro-, nano- and pico-plankton was also quantified from the compiled *in-situ* data in the same way as proportionality factor except using the quotient of NPP and $(\bar{E} \times \bar{a}_{PHY})$; see Table 3 for values; Barnes et al., 2014). The slope of the linear regression between NPP and $\bar{a}_{PHY}$, and NPP and $(\bar{E} \times \bar{a}_{PHY})$ could not be used as the slope coefficients were not significantly different to zero. The constant (1000) converts the estimate from mol C m$^{-3}$ d$^{-1}$ to mmol C m$^{-3}$ d$^{-1}$.

327

328 *2.7 Absorption model application*

329 The simplest absorption-based model (*NPP1*) was used to examine the dynamics of NPP in
330 two coastal locations using satellite products. Located in the tropical north-east and temperate
331 south-east of Australia, (Yongala and Port Hacking National Reference Stations,
332 respectively), these locations are fundamentally different in terms of their oceanographic
333 setting as well as average phytoplankton biomass, chlorophyll-*a* concentration and variability
334 (Jones et al., 2015; Lynch et al., 2014). However, each station is broadly representative of its
335 adjacent coastal waters (Jones et al., 2015) and thus serves as useful comparison in the
336 application of the absorption-based model to examine spatial and temporal differences of
337 NPP in Australian shelf waters.

338

339 Daily, 4 km, level 3 NASA MODIS Aqua phytoplankton absorption at 443 ($a_{PHY}$; $m^{-1}$),
340 derived from the generalised IOP default configuration model (GIOP-DC) and the most
341 recent processing (R2014) was obtained from the Ocean Biology Group at Goddard Space
342 Flight Centre for the years 2003-2015 (https://oceancolor.gsfc.nasa.gov/). Daily chlorophyll-
343 *a* (OC3 CHL; mg $m^{-3}$), sea surface temperature 4 micron (SST4; °C) and photosynthetically
344 active radiation (PAR; mol photons $m^{-2}$ $d^{-1}$) were also downloaded. The phytoplankton
345 absorption for PAR ($\bar{a}_{PHY}$) was empirically derived from the satellite value at 443 nm using
346 coefficients derived from the *in-situ* dataset: $\bar{a}_{PHY} = a_{PHY}(443) \times 0.3609 - 0.0005$ ($n =$
347 $41$; $R^2 = 0.97$).

348

349 The spatially averaged NPP of the surface layer (0 m) was computed for a ~ 50 km bounding
350 box (geometric mean of 12 x 12 pixel array) around the Yongala National Reference Station
351 (19°18.5 S, 147°37.1 E) and Port Hacking National Reference Station (34°05.0 S, 151°15.0

E) using *NPP1*. After inputting the relevant satellite products into equation 1, 8-day geometric mean composites were computed. The data was then log transformed (Campbell, 1995) and smoothed temporally with a three period (24 day) running mean to reduce high time frequency noise (Foukal and Thomas, 2014). The NPP anomaly was computed for each location by subtracting the geometric mean (Limpert et al., 2001; Yoder et al., 2002) across the full time-series from each time point and compared to the SST anomaly computed in the same way.

The absorption based primary productivity model *NPP1* was evaluated against the Chl-*a* based model, the Vertically Generalised Production Model (VGPM; Behrenfeld and Falkowski, 1997) for a single daily scene along the SE coast of Australia on the 18$^{th}$ of October, 2010, when a significant intrusion of warm water from the East Australian Current (EAC) into the Tasman Sea occurred. The VGPM was calculated as per Behrenfeld and Falkowski (1997) for the surface layer with the final value converted from mg C m$^{-3}$ d$^{-1}$ to mmol C m$^{-3}$ d$^{-1}$. The difference between NPP1 and VGPM was calculated as $(NPP1 - VGPM)$ ( Hirawake et al., 2011).

*2.6 Statistical assessments*

The relationship between measured NPP and $a_{PHY}$ ($\bar{a}_{PHY}$, $a_{PHY}$(440 nm) and $a_{PHY}$(676 nm); m$^{-1}$) was examined using type *II* linear regressions in *R* statistical package. Type *II* linear regressions, an ANCOVA comparison of slope coefficients, and the root mean square error (RMSE) were also used to evaluate the accuracy of the four absorption-based models (*NPP1*, *NPP2*, *NPP3* and *NPP4*) as compared to the *in-situ* observations.

376 To examine whether $\bar{a}_{PHY}$ varied predictably with other phytoplankton biological parameters
377 e.g. chlorophyll-*a* concentration, community composition, and physiology; biological data
378 (including NPP, TChl-*a*, $\bar{a}_{PHY}$, the proportion of photoprotective pigments in the total
379 pigment pool (PPC/TP), $\phi$, and the proportion of micro-, nano- and pico-plankton) from all
380 surface stations were analysed for similarities between stations. Non-metric Multi-
381 Dimensional scaling (MDS) and group average dendogram clustering were used to identify
382 clusters with at least 80 % similarity (Primer 6 and PERMANOVA+, Plymouth Marine
383 Laboratories, UK). Physico-chemical parameters (temperature, MLD, $K_d$(PAR), *E*, $NO_3$, $PO_4$,
384 Si and $NH_4^+$) were input into a multivariate distance based redundancy model (DistLM) as
385 predictors to explain the variability in the biological responses. Marginal tests were
386 conducted to examine how much variation in biological properties was explained by each
387 environmental variable. The BEST procedure was used to select the best solutions that
388 mapped the greatest variation in the biological parameters listed above (Clarke and Warwick,
389 2001).
390
391 To assess the dynamics in satellite absorption-modelled estimated NPP at Port Hacking NRS
392 and Yongala NRS, spatial averages, minimum and maximum NPP, and the annual timing
393 (week) of the maximum and minimum NPP were compared using Mann-Whitney *U* tests in *R*
394 statistical package. Kendall's tau correlations for non-normally distributed data tested the
395 relationship between the NPP anomaly and temperature anomaly.
396
397 **3. Results**
398 *3.1 Oceanographic conditions*
399 The voyages captured different physico-chemical conditions in Australian coastal waters
400 along the Northern and Eastern continental shelves. The highest values of surface salinity

were observed at PHNRS (35.6; Table 1) and the lowest at stations within the Great Barrier Reef where riverine influences were greatest (30.0; Table 1). Irrespective of the seasonal influences, stations sampled in Northern tropical waters were warmer, peaking at 31.4 °C in the North-west as compared to the substantially cooler surface waters in the sub-tropical South-east which experienced the lowest temperature of 20.1 °C (Table 1). Dissolved nitrate concentrations were typical of Australian tropical and sub-tropical waters, with increased surface values observed in the South-east close to the coastline (< 4.56 μmol $L^{-1}$; V2) and during winter sampling at PHNRS (< 1.89 μmol $L^{-1}$; Table 1). In contrast, silicate concentration peaked in the Northern Timor and Arafura Sea regions during V1 (4.00 μmol $L^{-1}$) and V3 (3.00 μmol $L^{-1}$; Table 1).

*3.2 Phytoplankton pigmentation, composition and NPP*

Total chlorophyll-*a* (TChl-*a*) concentration spanned 2 orders of magnitude (0.06-2.99 mg $m^{-3}$; Table 1), with the lowest measured TChl-*a* concentrations observed in the Coral Sea region during V3 in winter and the highest encountered during V2 in the South-east in spring. The proportion of the total phytoplankton pigment pool dedicated to photoprotective pigments (PPC/TP ratio) ranged between 3 and 24 % and was similar between regions, averaging 10 ± 1.0 % (Supplementary Table 1). Phytoplankton net primary productivity (NPP) and composition, inferred from pigments, was also variable. Phytoplankton NPP (Figure 2) was spatially variable, ranging from 0.2 to 19.3 mmol C $m^{-3}$ $d^{-1}$ (Table 1; Figure 2). However, increased NPP rates were generally observed at stations where microplankton specific pigments (fucoxanthin and peridinin) dominated the diagnostic pigment biomass (Figure 2, Supplementary Table 1). The observed NPP generally decreased as the community structure changed from being microplankton dominated to picoplankton dominated (Figure 2, Supplementary Table 1).

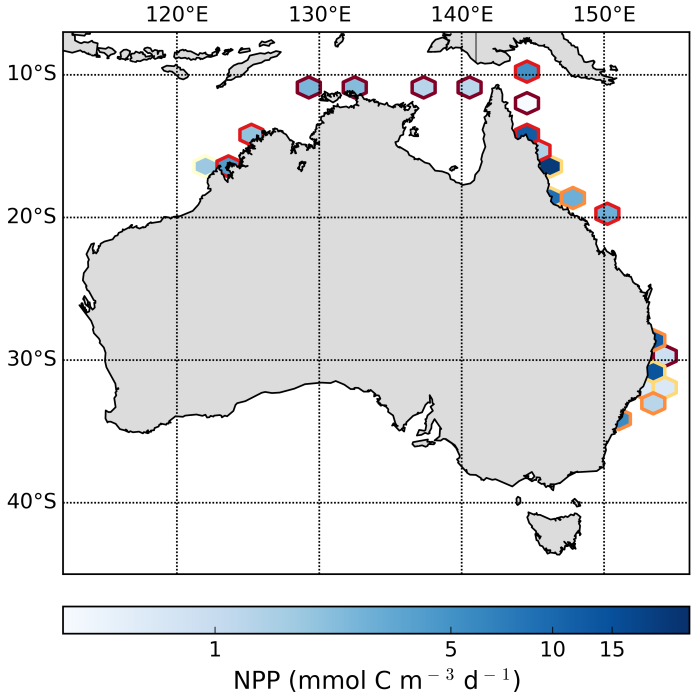


Figure 2. Observed NPP at each station, measured using $^{13}C$ or $^{14}C$ (symbol fill colour). The symbol border represents the dominant size class of phytoplankton within each sample (See section 2.2.4): yellow = mixed community, orange = picoplankton, red = nanoplankton, maroon = microplankton dominated.

*3.3 Optical properties*

Attenuation of available light in the surface layers around the coast was highly variable during all voyages. The diffuse light attenuation coefficient ($K_d$(PAR)) ranged from 0.04 to 0.49 $m^{-1}$ (Table 2). Total absorption of available light at 440 nm ($a_{PHY}$ + $a_{NAP}$ + $a_{CDOM}$) varied between 0.01-1.8 $m^{-1}$, increasing at stations closer to the coast (Table 2). CDOM was the dominant measured optically-active constituent, contributing to 50 % or more of the total absorption in 75 % of samples (Table 2; Figure 3). Light absorption by phytoplankton $a_{PHY}$(440 nm) varied between 0.008 and 0.142 $m^{-1}$ (Table 2), and showed a general trend of increasing inversely with $a_{CDOM}$(440 nm). However, phytoplankton dominated the particulate ($a_{PHY}/a_{PART}$(440 nm) absorption at most stations (Table 2; Figure 3) and there was a significant covariation between $a_{PHY}$(440 nm) and $a_{NAP}$(440 nm), with $a_{NAP}$ increasing

according to a power function ($a_{nap}(440\ nm)=3.3809[a_{PHY}(440\ nm)]^{1.6313}$; $R^2$ = 0.56). The spectral dependencies of light absorption by CDOM and NAP (spectral slopes $S_{CDOM}$ and $S_{NAP}$) were variable spatially and showed no covariance with the respective absorption coefficients at 440 nm ($a_{CDOM}(440\ nm)$ and $a_{NAP}(440nm)$; Table 2).

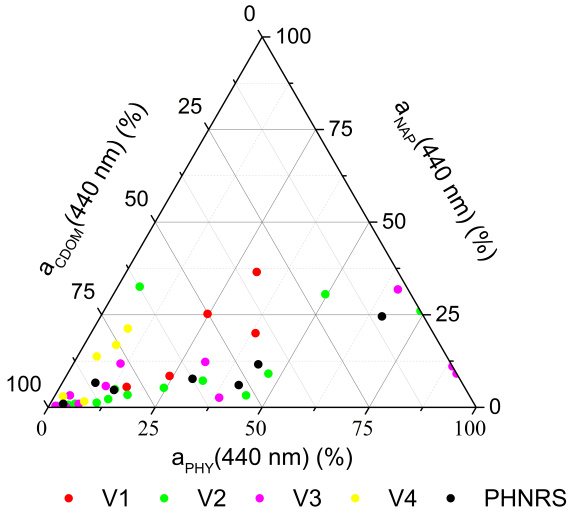


Figure 3. Light absorption budget for each station and percentages of light absorption at 440 nm attributed to phytoplankton (x=$a_{PHY}$), coloured dissolved organic matter (y=$a_{CDOM}$) and non-algal Particulates (z=$a_{NAP}$).

*3.4 Phytoplankton absorption as a predictor of NPP*

The phytoplankton absorption coefficient for PAR ($\bar{a}_{PHY}$) was linearly related to NPP and could explain 71 % of the variability in NPP ($R^2$ = 0.71, $n$=41, $p$<0.05; Table 3, Figure 4). The absorption coefficient at 676 nm was similarly related to NPP ($a_{PHY}(676\ nm)$; $R^2$=0.70, $n$=41, $p$<0.05), but there was a somewhat weaker relationship between the NPP and $a_{PHY}(440$ nm) ($R^2$=0.65, $n$=41, $p$<0.05; Table 3). The proportionality factor ($p$; slope of $\bar{a}_{PHY}$ vs NPP) for the whole dataset was 304 (as compared to 510 for Marra et al. (2007)) and the average quantum yield ($\phi$; slope of $(\bar{E} \times \bar{a}_{PHY})$vs NPP) was 0.025 ±0.004 (S.E.) mol C mol photons$^{-1}$.

463 Multivariate analyses revealed $\bar{a}_{PHY}$ and NPP varied in a similar fashion with phytoplankton
464 chlorophyll-*a* concentration, community structure and physiology (Supplementary Table 1).
465 There was > 80 % within cluster similarity (Bray-curtis resemblance, $p < 0.05$; Figure 4) in
466 TChl-*a*, $\bar{a}_{PHY}$, $\phi$, PPC/TP, dominant size class and the NPP properties of three distinct
467 clusters of stations. The NPP, $\bar{a}_{PHY}$, TChl-*a* concentration, proportion of microplankton and
468 quantum efficiency decreased in samples moving from cluster 1 to cluster 3. Samples in
469 cluster 3 had the lowest $\bar{a}_{PHY}$ coefficients but highest proportion of picoplankton in the
470 community and highest proportion PPC pigments (Supplementary Table 1). The individual
471 traits of each cluster are summarised in Supplementary Table 1.
472
473 The multivariate distance based redundancy model (DistLM) indicated that environmental
474 parameters together (temperature, MLD, $K_d$(PAR), *E*, $NO_3$, $PO_4$, Si and $NH_4^+$) could explain
475 64 % of the variation in phytoplankton biological parameters (NPP, TChl-*a*, $a_{PHY}$, $\phi$, PPC/TP
476 and dominant size class) and subsequently the separation of biological clusters identified
477 earlier. The variables $K_d$(PAR), nitrate and phosphate were significant individual drivers
478 (marginal tests $p < 0.05$; Supplementary Table 2,
479 Supplementary Figure 1) and together could explain 65 % of the variability in phytoplankton
480 NPP and biology (BEST solutions $R^2 = 0.65$; Supplementary Table 3). Pearson's correlation
481 coefficients (correlations > 0.5) and pairwise tests revealed that cluster 1 (high NPP) was
482 significantly correlated with increasing nitrate and phosphate concentration, whereas cluster 2
483 (medium NPP) responded to increasing silicate and light attenuation ($K_d$(PAR)). Cluster 3
484 (low NPP) experienced reduced nutrient concentrations (nitrate, phosphate and silicate),
485 increased light penetration (low $K_d$) and shallower MLDs.
486

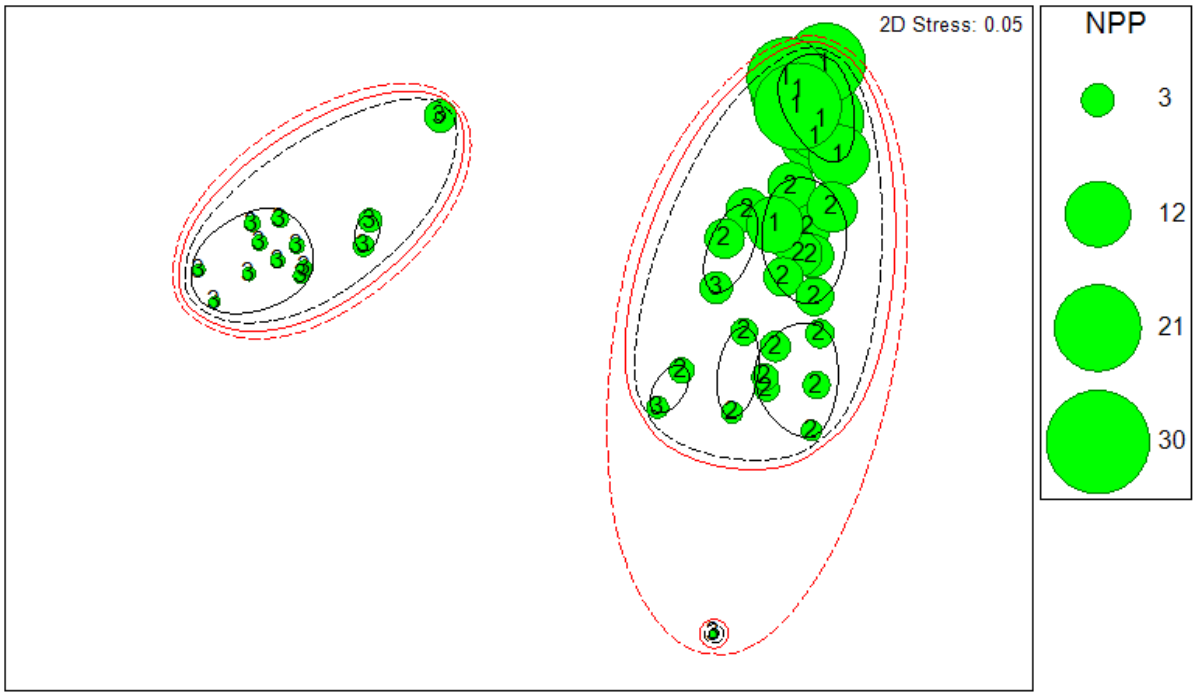


487

488 Figure 4. Multi-dimensional scaling plot of *in-situ* biological data collected at each station
489 (including NPP, TChl-*a*, $\bar{a}_{PHY}$, PPC/TP and proportion of microplankton, nanoplankton,
490 picoplankton) revealing three distinct clusters (at least 80% within cluster similarity) that
491 partition based on level of NPP (mmol C $m^{-3}$ $d^{-1}$; green symbols). Lines indicate level of
492 similarity between samples based on a group average cluster dendogram, with similarity set
493 at 90 % (solid black), 80 % (dashed black), 70 % (red solid) and 60 % (red dashed). Numbers
494 1-3 indicate biological cluster, with NPP decreasing from cluster 1 to cluster 3.
495

496 All four absorption-based models, *NPP1*, *NPP2*, *NPP3* and *NPP4* could reliably estimate
497 NPP (Figure 5). However, there were no significant difference between the models in the
498 variability of NPP explained ($R^2$ ~ 0.73), the deviation of the slopes from the 1:1 relationship
499 between the model and the observations ($F_{(2,102)}$=0.702, $p$ > 0.05; see Table 3 for linear
500 relationships), or the root mean square error (RMSE ~ 2.4; See Table 3 for all parameters).
501

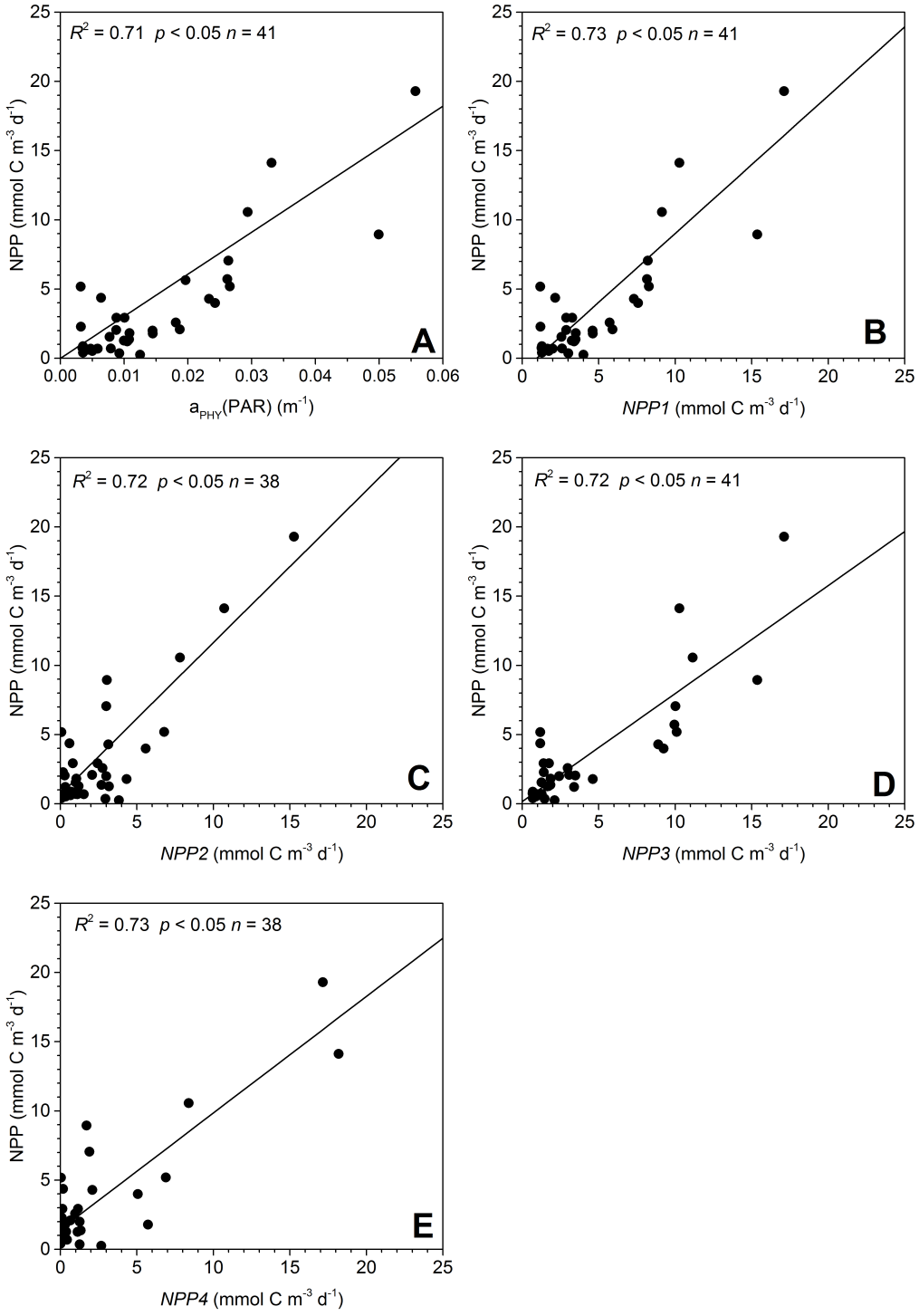


Figure 5. Comparisons between NPP and the (A) spectrally integrated absorption coefficient $\bar{a}_{PHY}$, (B) *NPP1* (Eqn. 1. proportionality factor), (C) *NPP2* (Eqn. 2. fixed quantum efficiency), (D) *NPP3* (Eqn. 3 size class specific proportionality factor) and (E) *NPP4* (Eqn. 4. size class specific quantum efficiency).

508 *3.7 Dynamics of NPP at locations on the Australian east coast*

509 To demonstrate the dynamic range and sensitivity of the absorption-based model, the
510 simplest absorption model (*NPP1*) and a chlorophyll-based model (VGPM) were applied in a
511 region of the East Australian Current on the east coast of Australia. MODIS SST
512 observations of this region on 18 October 2010 (Figure 6A) show significant mesoscale
513 variability in water mass features along the south-east coast of Australia, capturing the
514 intrusion of warm oligotrophic waters of the East Australian current (EAC) into the southern
515 Tasman Sea region. Separation of the EAC is observed around 30° S which often facilitates
516 the formation of cold-core eddies offshore. Nutrient-dense cold water uplift (~ 19 °C) is
517 observed along the coastline between 32° S and 34° S and fingers of cooler Tasman Front
518 waters can be seen moving north-east from 32° S 152° E. The *NPP1* model produced on
519 average higher estimates of spatially averaged daily NPP (mean difference *NPP1*-VGPM
520 1.45 mmol C $m^{-3}$ $d^{-1}$, Figure 6D; *NPP1* mean 1.66 mmol C $m^{-3}$ $d^{-1}$) as compared to the
521 VGPM (mean 0.78 mmol C $m^{-3}$ $d^{-1}$). However, the minimum and maximum modelled values
522 produced by the VGPM were higher (0.03 and 22.8 mmol C $m^{-3}$ $d^{-1}$), and extremely high
523 values fringed the coastlines (Figure 6C). In contrast, the absolute minimum and maximum
524 values produced by the *NPP1* were lower (0.001 and 19.7 mmol C $m^{-3}$ $d^{-1}$), and the highest
525 values featured in areas where the differential in temperature between adjacent water masses
526 was greatest (Figure 6A & B).

527

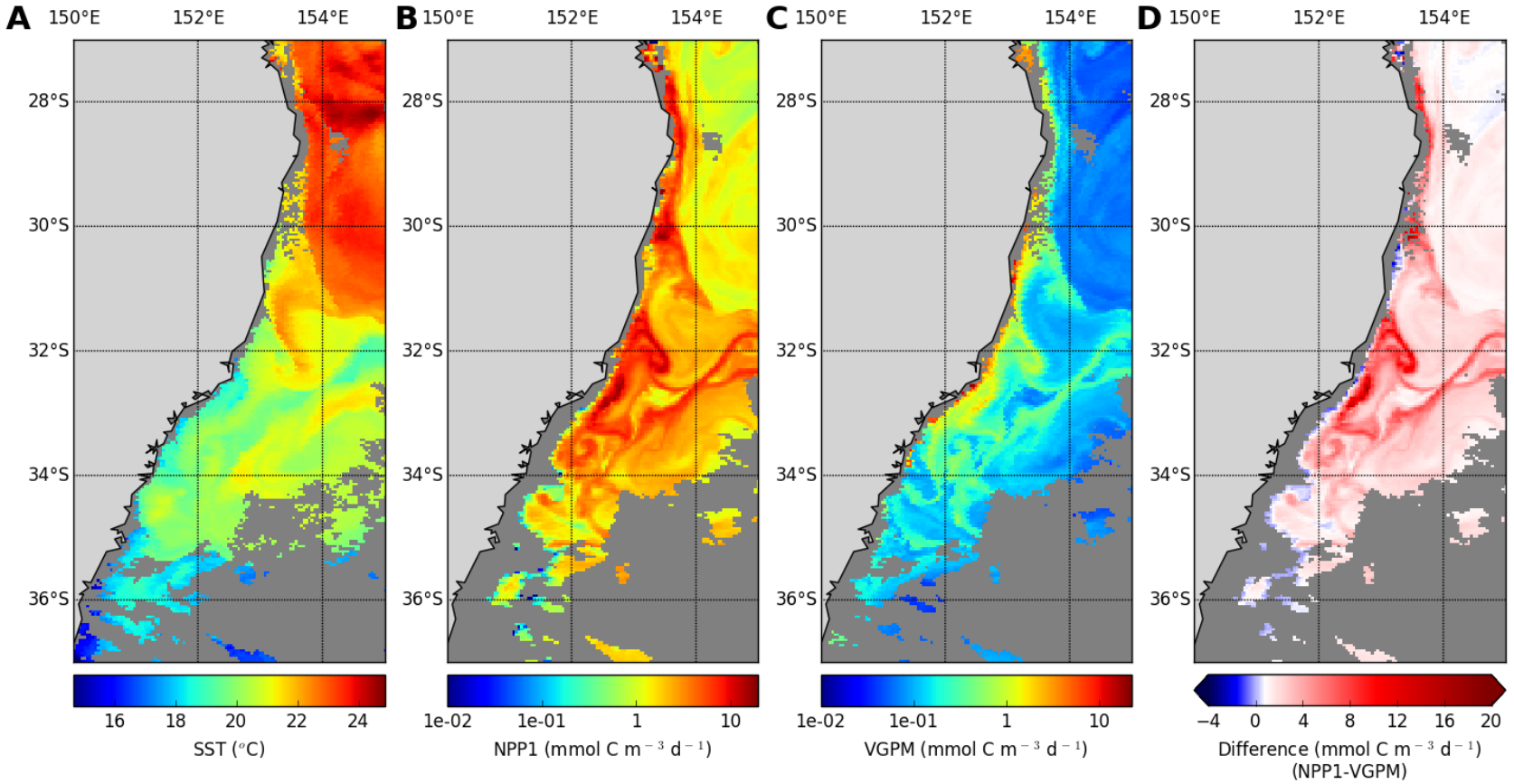


528

529 Figure 6. Evaluation of the NPP1 absorption model against the VGPM model using the MODIS Aqua scene from the 18 October 2010. Plots
530 show a significant intrusion of warm water from the Eastern Australian Current into temperate waters (**A**; SST). Surface NPP has been
531 calculated using the NPP1 (**B**), VGPM (**C**) and the difference in NPP derived by the NPP1 and VGPM models (**D**).
532

533 *NPP1* was applied to estimate daily spatially averaged NPP at Yongala and Port Hacking
534 National reference stations between 2003 and 2013. The model applied to the satellite
535 $a_{PHY}(443)$ product produced estimates within the range observed *in-situ* in this compiled
536 dataset and the literature (Figure 7). According to the *NPP1* absorption-based model, the
537 mean surface NPP throughout the entire time-series was significantly higher at Port Hacking
538 (1.71 ± 0.03 (S.E.) mmol C $m^{-3}$ $d^{-1}$; $U = 14$, $n=13$, $p < 0.05$) than at Yongala (1.43 ± 0.03
539 (S.E.) mmol C $m^{-3}$ $d^{-1}$; Figure 8A and B). The average annual minimum (PH: 0.85 mmol C
540 $m^{-3}$ $d^{-1}$ and YONG: 0.79 mmol C $m^{-3}$ $d^{-1}$) and annual maximum (PH: 3.28 mmol C $m^{-3}$ $d^{-1}$ and
541 YONG: 2.92 mmol C $m^{-3}$ $d^{-1}$) values at each location did not differ ($p > 0.05$). However, the
542 timing of the annual NPP maximum occurred significantly earlier in the year at Yongala NRS
543 (median week = 11; mean ± S.E. = 10.77±3.32) than at Port Hacking NRS (median week =
544 26; mean ± S.E. = 26.07±1.74; $U= 0$, $n=13$, $p < 0.05$). Inter-annual variability in the timing of
545 the NPP minimum was greater, and the timing of the annual minimum NPP was not
546 significantly different between Yongala (median week = 34; mean ± S.E. = 29.85±7.66) and
547 PHNRS (median week = 9; mean ± S.E. = 11.77±4.76; $U= 63$, $n=13$, $p > 0.05$).
548
549 Temporal anomalies in the surface NPP were correlated to sea surface temperature in both
550 locations (Figure 8C and 8D). NPP increased with the SST anomaly at Yongala ($z=12.159$,
551 Kendall's $\tau=0.33$, $p < 0.05$; Figure 8C), but an inverse relationship between SST and NPP
552 anomalies was apparent at Port Hacking ($z=-15.422$, Kendall's $\tau=-0.42$, $p <0.05$; Figure 8D).

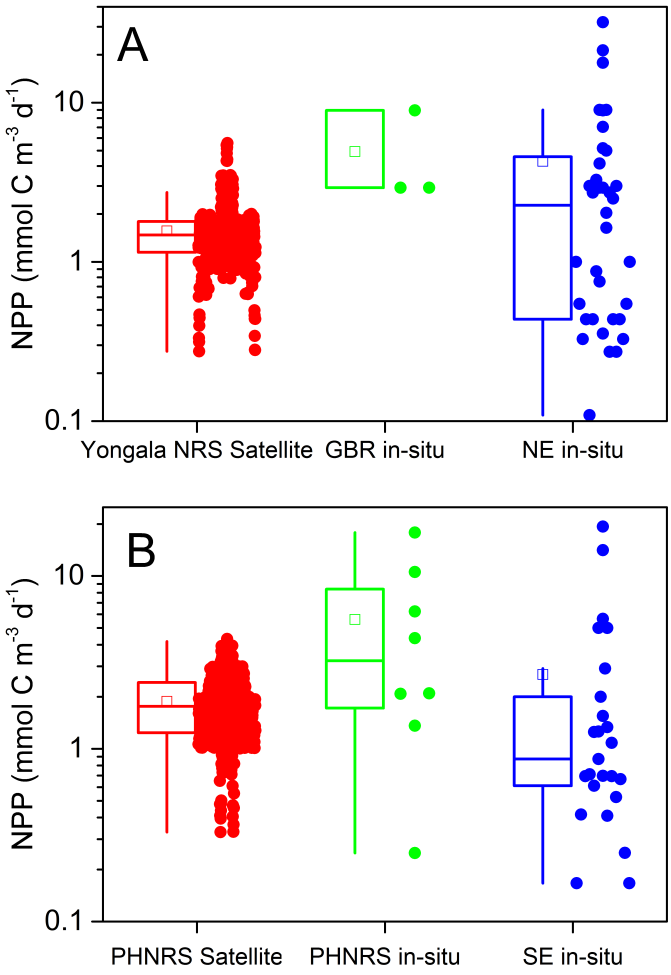


553
554 Figure 7. Comparison of satellite estimates of NPP using the absorption-based model *NPP1*
555 (red) and *in-situ* observations of NPP measured using $^{13}C$ and $^{14}C$. *In-situ* data was compiled
556 from this dataset and the literature (Everett and Doblin, 2015; Furnas and Carpenter, 2016;
557 Furnas and Mitchell, 1987; Glibert et al., 2006) for locations within the PH NRS and Yongala
558 NRS 50 km bounding box (green) and along the North-east (NE) and South-east (SE)
559 coastlines (blue).

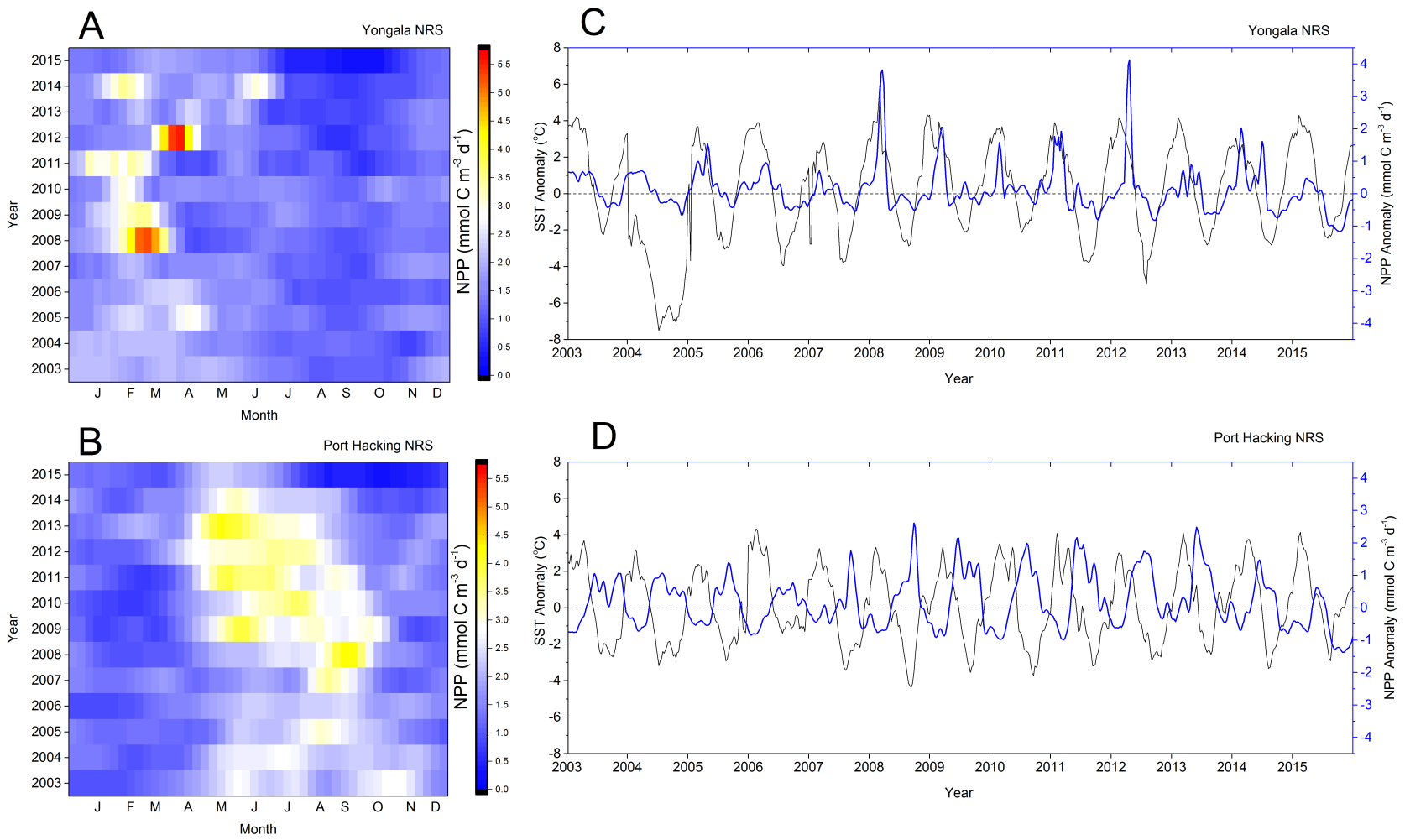


Figure 8. Comparison of the seasonal and inter-annual variability of NPP (**A** and **B**), as well as NPP and SST anomaly (**C** and **D**) all derived from satellite products at the Yongala and Port Hacking National Reference Stations (NRS; 12 x 12 pixel spatial average) for 2003 to 2015. Anomalies were calculated by subtracting the geometric mean across the time series (2003-2015) from each time point observation.

564 **4. Discussion**

565 The phytoplankton bio-optical property, the absorption coefficient has been extensively used
566 to predict primary productivity in the open ocean (Aiken et al., 2008; Barnes et al., 2014;
567 Marra et al., 2007). The dynamic range and error in satellite algorithms retrieving the
568 phytoplankton absorption coefficient are significantly better than that of the best performing
569 chlorophyll retrievals in optically complex coastal waters. However, the evaluation and
570 application of an absorption-based model has had limited attention in coastal waters,
571 including all tropical to temperate waters of the Southern Hemisphere, including around
572 Australia (Lee et al., 1996; Barker et al., 2007; Shang et al., 2010; Hirawake et al., 2011). In
573 this study, we evaluated four common forms of an absorption-based model using a
574 moderately sized dataset from coastal Australia. Each model explained 73% of the observed
575 surface NPP, and demonstrated near 1:1 observation-model correspondence. Application of
576 the simplest absorption-based model *NPP1* demonstrated distinctly different dynamics in
577 surface NPP at two locations within the East Australian continental shelf.
578

579 **Phytoplankton absorption model predicts NPP**

580 Sampling across a wide range of physico-chemical environments and phytoplankton
581 chlorophyll concentrations (0.06 – 2.99 mg Chl-*a* $m^{-3}$) demonstrated that the phytoplankton
582 absorption coefficient (spectrally averaged and at 676 nm) was directly related to changes in
583 carbon fixation and environmental conditions. The availability of essential nutrients and light
584 at the sampling stations played a major role in the composition of the phytoplankton
585 communities, selecting for particular ecological and bio-optical traits (Aiken et al., 2008;
586 Lavaud et al., 2007). This is consistent with observations in other oceanic waters (e.g. Aiken
587 et al. (2008)), and observations of latitudinal shifts in phytoplankton biomass and community
588 composition (Burford et al., 2009; Hayes et al., 2005) around Australia's coastline, driven by

589 distinct changes in physical conditions e.g. dissolved nutrients and temperature (Condie and
590 Dunn, 2006). At stations with low dissolved nitrate, phytoplankton biomass was relatively
591 low, dominated by nano- and pico-phytoplankton with low $a_{PHY}$, whereas increased dissolved
592 nutrients enhanced NPP and led to the dominance of microplankton. We also found that an
593 increase in photoprotective pigments relative to the total pigment pool (i.e., PPC/TP) and
594 increased daily irradiance resulted in reduced $a_{PHY}$ and NPP. This suggests a light driven
595 increase in PPC concentrations and hence lower quantum efficiencies and lower NPP rates,
596 due to the dissipation of excess light energy away from photosystems (Brunet and Lizon,
597 2003).
598
599 It is clear from both *in-situ* observations and satellite estimates of NPP that the dynamic
600 range of daily phytoplankton NPP rates in this study is consistent across locations from the
601 North-west to the South-east of the Australian coast, however the seasonality is distinctly
602 different between locations. *In-situ* observations and satellite ($a_{PHY}$ derived) estimates of
603 surface NPP were comparable to those reported (for $^{13}C$ and $^{14}C$ incubations) in the literature
604 for the North-west Kimberley region and in the North (0.6-8 mmol C $m^{-3}$ $d^{-1}$; Furnas and
605 Carpenter, 2016 and references therein), GBR (0.2-4.1 mmol C $m^{-3}$ $d^{-1}$; Furnas and Carpenter,
606 2016; Furnas and Mitchell, 1987) and South-east (0.1-5 mmol C $m^{-3}$ $d^{-1}$; Everett and Doblin,
607 2015; See also Figure 7). We observed the highest *in-situ* daily NPP rates at stations in the
608 South-east (V2 and PHNRS) and expected that the mean *in-situ* daily NPP would also peak in
609 this region (Everett and Doblin, 2015) given the propensity for wind-driven and EAC driven
610 upwelling (Roughan and Middleton, 2002) which encourages the growth of nanoplankton and
611 microplankton (Ajani et al., 2014; Kelly et al., 2015). Generally, the oligotrophic Coral Sea
612 region of the North-east supports very low phytoplankton biomass (Hayes et al., 2005). But
613 instead, the mean *in-situ* daily NPP was highest in the GBR, likely because of a low sample

614 count and the fact that sampling occurred after extreme rainfall brought on by Tropical
615 Cyclone Oswald in January 2013 (Johnson et al., 2013), delivering nutrient enriched inflows
616 into the generally nutrient limited reef (Furnas, 2003). When the sample size for NPP
617 observations is increased at Yongala and Port Hacking National Reference Stations (NRS),
618 by estimating the satellite derived NPP, the mean *in-situ* daily NPP across the 2003-2013
619 satellite record was higher at the south-east location than the north-east.
620
621 The timing of maximum daily phytoplankton NPP occurs in March at Yongala and July at
622 Port Hacking NRS, and appears to correlate with seasonal temperature anomalies. At
623 Yongala, a tropical monsoon climate during the austral wet season (November-March)
624 creates warmer water temperatures and high rainfall (Condie and Dunn, 2006; Hayes et al.,
625 2005). The rainfall discharges large nutrient and dissolved and particulate organic carbon
626 loadings into the inner reef lagoon increasing phytoplankton chlorophyll concentration
627 (which also peaks in March; Blondeau-Patissier et al., 2011) and phytoplankton productivity
628 (Devlin and Brodie, 2005). Waters at Port Hacking were long thought to experience austral
629 spring blooms (Dakin and Colefax, 1940, 1933; Hayes et al., 2005) more characteristic of
630 temperate waters further south (36 °S to 48 °S; Condie and Dunn, 2006; Thompson et al.,
631 2009). In contrast, our results show that NPP peaks during winter at Port Hacking, when
632 cooling waters create deeper mixed layer depths (Everett and Doblin, 2015) and have higher
633 dissolved nitrate concentrations (Kelly et al., 2015). Chlorophyll-*a* concentration, although
634 not always synchronous with NPP, is also negatively correlated to *in-situ* water temperature,
635 and winter and spring concentrations have been shown to be comparable (Everett and Doblin,
636 2015; Kelly et al., 2015).
637

638 **Examination of uncertainty in the absorption model**

639 Four common forms of an absorption-based model were compared to *in-situ* observations of
640 NPP and each presented ~30 % uncertainty in the estimates of NPP. There are a number of
641 known limitations to the use of phytoplankton absorption parameter to estimate NPP,
642 including the influence of pigment composition, species composition, cell sizes and
643 environmental history on $a_{PHY}$ and other terms in the models (Bricaud et al., 2004; Lee et al.,
644 2015; Marra et al., 2007). Where possible we have attempted to reduce those uncertainties.
645 We used the $\bar{a}_{PHY}$ parameter, rather than $a_{PHY}(440\ nm)$ which was sensitive to changes in
646 photoprotective pigment concentrations and pigment packaging (Supplementary Figures 2-4),
647 whereas the $\bar{a}_{PHY}$ was not. Marra et al. (2003), Hirata et al. (2008) and Lee et al. (1996)
648 suggested that better parameterisation of the maximum phytoplankton quantum efficiency
649 ($\phi_m$) or proportionality factor ($p$), would increase the accuracy of absorption-based models.
650 Compared to the global averages of $p$ (relationship between NPP and $\bar{a}_{PHY}$; 510 in Marra et
651 al. (2003)) and the maximum quantum yield ($\phi_m$; 0.06 mol C mol photons$^{-1}$ in Marra et al.
652 (2003)), our values of $p$ and $\phi_m$ were low (304 and 0.025 respectively) although within
653 values reported for temperate and sub-tropical waters (Oliver et al., 2004). Our application of
654 the regionally derived $p$ in *NPP1* and size-based parameterisations of $p$ and $\phi_m$ in *NPP3* and
655 *NPP4* respectively, did not reduce the overall uncertainty. The relationship between
656 phytoplankton cell size and quantum efficiencies is still contended in the literature (Aiken et
657 al., 2008; Bouman et al., 2000; Cermeño et al., 2005; Finkel, 2001; Robinson et al., 2014).
658 However specific examples do highlight that the availability of light and nutrients plays an
659 important role in both the selection of cell size, and the photosynthetic rates of those cells.
660 For example, in some coastal environments under high nutrient and adequate light conditions,
661 larger phytoplankton such as microplankton display higher photosynthetic efficiencies (Aiken
662 et al., 2008; Cermeño et al., 2005; Giannini and Ciotti, 2016; Robinson et al., 2014; Uitz et

663 al., 2008). Uitz et al. (2008) contend that in stable, oligotrophic, high-light conditions,
664 smaller cells can achieve balanced growth and higher photosynthetic efficiencies than larger
665 cells that may be stressed under the same conditions. In order to reduce uncertainties, it is
666 likely that $p$ or $\phi$ need to be parameterised according to community structure and
667 environmental conditions, and at the very least in high nutrient / adequate light, and low
668 nutrient / stressful light conditions.
669
670 The value selection and treatment of light terms $K_\phi$ and $\bar{E}$, and normalisation of $\bar{E}$ using
671 ($\bar{a}_{PHY}/\bar{a}_{TOT}$ i.e. calculation of *APAR*) may also introduce error into *in-situ* models and the
672 computation of the size-based quantum efficiencies. The saturation threshold ($K_\phi$) dependent
673 on the phytoplankton species present and their environmental light history (Hanson et al.,
674 2007; Kiefer and Mitchell, 1983; Suggett et al., 2006). The $K_\phi$ value of 10 mols photons $m^{-2}$
675 $d^{-1}$ (≈ 230 μmol photons $m^{-2}$ $s^{-1}$; Kiefer and Mitchell, 1983) is a good approximation for the
676 saturation irradiance for Australian continental shelf waters (Hanson et al., 2005; Kirk, 2011)
677 and is within the global upper limit (Silsbe et al., 2016). The satellite daily PAR ($\bar{E}$) is
678 susceptible to errors due the use of the global atmospheric correction and when the parameter
679 is used at daily time steps as opposed to a 8-day composite (Patt et al., 2003). Any small
680 measurement errors in the determination of $\bar{a}_{PHY}$ or $\bar{a}_{TOT}$ will be reintroduced in the
681 normalisation of $\bar{E}$ (Frouin and Kampel, 2014). However, given that phytoplankton were
682 overwhelmingly outcompeted by CDOM for light at 440 nm, the correction for the removal
683 of available light by non-phytoplankton in-water constituents is important to ensure that the
684 available light is not overestimated.

685 **Potential for further application of an absorption-based satellite model in Australian**
686 **waters**

687 The absorption-based model *NPP1* captured spatial and temporal dynamics in NPP within
688 waters which represent moderate chlorophyll-low variation and high chlorophyll-high
689 variation conditions, and hydrodynamic features such as counter currents and nutrient
690 upwellings which are common to Australian shelf waters (Figure 6; Hanson et al., 2005;
691 Jones et al., 2015; van Ruth et al., 2010). Ma et al. (2014) and Foukal and Thomas (2014)
692 demonstrated that absorption-based models were sensitive to spatial patterns in NPP and
693 produced reliable seasonal trends in NPP when applied in coastal regions, particularly where
694 upwelling features were present. The NPP seasonal cycle obtained from the *NPP1* model at
695 Yongala and Port Hacking National Reference Stations conformed with our expectations of
696 NPP dynamics and physical processes controlling phytoplankton at these locations.
697 According to Jones et al. (2015) biological processes observed at Port Hacking and Yongala
698 NRS are representative of areas across the continental shelf as large as 37 746 $km^2$ and 185
699 490 $km^2$ respectively. Relative to the chlorophyll-based VGPM model, the *NPP1* model was
700 more sensitive to temperature changes between water masses and sub-mesoscale features in a
701 region of optically complex waters along the South East Australian Coast (Figure 6). As
702 expected, NPP generally increased in frontal areas of mixing where the more productive
703 Tasman Sea interacted with the warm oligotrophic EAC waters (Everett et al., 2014;
704 Roughan and Middleton, 2002). Similar to Everett et al. (2015) the VGPM model
705 overestimated NPP along the coast and underestimated NPP in the EAC regions offshore
706 compared to *NPP1*.
707
708 This study tested the utility of the absorption-based model in surface waters only, but in areas
709 along the Western Australian coast (Hanson et al., 2007) and Southern Great Australian Bight

710 (van Ruth et al., 2010) a high proportion of the water-column phytoplankton biomass and
711 productivity is contained within deep chlorophyll layers. Deep chlorophyll maxima are
712 frequent features within the Coral Sea and East Australian Current but are not usually major
713 contributors to water column NPP (Hassler et al., 2011; Hayes et al., 2005). Depth-resolved
714 absorption-based NPP models have been used successfully in the Western English Channel
715 (Barnes et al., 2014), North Sea (Bouman et al., 2010) and Southern Ocean (Shang et al.,
716 2010). The Ocean Productivity Database (Marra et al., 2016) indicates that from polar to
717 tropical oceans, $\bar{a}_{PHY}$ is a very good predictor of NPP within the first optical depth ($\xi$), which
718 depending on location, represents depths of 1.7-29 m (if $\xi = 1/K_d(PAR)$) or the uppermost 4-
719 90 % of the mixed layer for the waters sampled within this study.
720
721 The satellite phytoplankton absorption coefficient was derived from the Generalised IOP DC
722 model which has demonstrated a high percentage (> 80 %) of valid retrievals of $a_{PHY}$ in
723 waters of all trophic levels and across all seasons (Werdell et al., 2013). Although the GIOP
724 DC was applied to optically complex waters (Cherukuru et al., 2016; Oubelkheir et al., 2014)
725 and without local atmospheric correction, the GIOP-DC uncertainty product for $a_{PHY}(443)$
726 indicates generally low uncertainty across the 2003-2015 time-series of $a_{PHY}(443)$ retrievals
727 at Port Hacking and Yongala NRS. Within the 589 weeks of $a_{PHY}(443)$ observations at Port
728 Hacking NRS, 43 weeks demonstrated uncertainty > ±0.005 $m^{-1}$, of which 4 weeks the
729 uncertainty was > ±0.01 $m^{-1}$. In comparison at Yongala NRS, of 570 weeks of data, 46 weeks
730 of observations had uncertainties of > ±0.005 $m^{-1}$ with 19 weeks > ±0.01 $m^{-1}$. Observations of
731 high uncertainty (> ±0.01 $m^{-1}$) at Yongala NRS included periods when $a_{PHY}$ and hence NPP
732 were high, between mid-February to mid-March 2008 and mid-March to mid-April 2012.
733 During this time, increased wet-season land-flows deliver high concentrations of CDOM and

734 total suspended material into the GBR region, which are likely to interfere with satellite
735 retrievals of IOPs (Hayes et al., 2005; Oubelkheir et al., 2014), but the same conditions can
736 also contribute to local upwelling and delivery of nutrients, increasing $a_{PHY}$ and NPP (Devlin
737 and Brodie, 2005; Hayes et al., 2005).
738
739 Qin et al. (2007) demonstrated that semi-analytical algorithms (SAAs) applied in the GBR
740 region are highly sensitive to increasing concentrations of NAP and CDOM, however Brando
741 et al. (2012) show that the error can be minimised with regionally specific IOPs and SIOPs.
742 We found no spatial trends in the IOP and SIOPs for phytoplankton, NAP and CDOM or co-
743 variation in spectral slopes with absorption coefficients which could be used to parameterise
744 the spectral shapes in SAAs. Like other studies, we find CDOM to be the dominant measured
745 optically active constituent (Cherukuru et al., 2014; Clementson et al., 2004); but did not
746 observe relationships between $a_{CDOM}$ and physical properties (e.g. salinity), or $a_{CDOM}$ and
747 $S_{CDOM}$, which can be used to discern the source and concentration of CDOM (Andrew et al.,
748 2013; Del Vecchio and Blough, 2002; Green and Blough, 1994). In contrast to studies
749 focused on riverine outputs in Tasmania (Cherukuru et al., 2014; Clementson et al., 2004)
750 and within the tidally dynamic GBR (Blondeau-Patissier et al., 2009; Oubelkheir et al.,
751 2006), in this study phytoplankton dominated the particulate absorption and were likely
752 major contributors to the detrital particulate fraction. The Australian Commonwealth
753 Scientific and Industry Research Organisation maintains the Australian-waters Earth
754 Observation Phytoplankton-type Products (AESOP) database, a global standard database of
755 IOPs from Australian waters, which could be used to develop better parameterisations of
756 IOPs and SIOPs for regionally-tuning SAAs and testing atmospheric corrections around the
757 entire Australian coastline.
758

## Conclusion

Primary productivity in Australian continental shelf waters varies with phytoplankton absorption. An absorption-based model explained 73% of the variation in surface NPP in Australian coastal waters when applied to datasets spanning two orders of chlorophyll-*a* concentration (0.60 – 2.99 mg Chl-*a* $m^{-3}$) and net primary productivity rates from 0.20 to 19.3 mmol C $m^{-3}$ $d^{-1}$. Overall, the spectrally averaged absorption coefficient $\bar{a}_{PHY}$ was a good first order predictor for NPP and varied in response to the environment in a similar fashion to NPP. Inclusion of a sized based parametrisation of the quantum efficiency and proportionality factor (slope of $\bar{a}_{PHY}$ and NPP) made little difference to the model performance. But this approach could be improved with additional *in-situ* coupled measurements of NPP and phytoplankton absorption, including discrete-depth sampling. Application of the absorption model to the GIOP-DC satellite $a_{PHY}$ product revealed different seasonality of NPP at Yongala and Port Hacking NRS. There is opportunity to improve the validity of satellite $a_{PHY}$ retrievals by using the existing AESOP database to regionally tune and atmospherically correct SAAs within the GIOP framework. An absorption-based model to estimate NPP is a promising approach for exploring the spatio-temporal dynamics in phytoplankton NPP around the entire Australian continental shelf.

## Acknowledgements

The authors would like to thank M. Alvarez for providing primary productivity data from PHNRS, and L. Clementson for providing absorption coefficients and HPLC data for V1, V2 and V4 and for training C. M. Robinson in particulate absorption measurements. We thank the scientific participants, captain and crew of the Marine National Facility *RV* Southern Surveyor, James Cook University *RV* James Kirby and Zelda Faith II for their assistance and support with sample collection. We appreciate the efforts of the NASA Ocean Biology

784 Processing Group for the continued provision of MODIS Aqua satellite data. We also thank
785 L. Mesarova for her assistance running the HPLC samples, the University of Technology
786 Sydney Microstructural Analysis Unit for technical support and instrumentation and the
787 Sydney Institute of Marine Sciences for the provision of instruments for optical
788 measurements. The Australian Integrated Marine Observing System is supported by the
789 Australian Government through the National Collaborative Research Infrastructure Strategy
790 and the Super Science Initiative. This research was supported under the Australian Research
791 Council's Discovery Projects funding scheme (DP1092892 and DP140101340 awarded to M.
792 A. Doblin). C. M. Robinson is supported by a CSIRO (2012010157) Australia Wealth from
793 the Oceans Flagship top-up scholarship and a UTS Plant Functional Biology and Climate
794 Change Cluster scholarship. This research forms part of the CSIRO funded Marine and
795 Coastal Carbon Biogeochemistry Cluster and C. M. Robinson's thesis. The authors appreciate
796 the comments provided by M. Baird and D. Blondeau-Patissier, and an anonymous reviewer
797 who helped to improve the manuscript.

798

799 **References**

800 Aiken, J., Hardman-Mountford, N.J., Barlow, R., Fishwick, J., Hirata, T., Smyth, T., 2008.
801 Functional links between bioenergetics and bio-optical traits of phytoplankton
802 taxonomic groups: An overarching hypothesis with applications for ocean colour remote
803 sensing. J. Plankton Res. 30, 165–181. doi:10.1093/plankt/fbm098

804 Ajani, P.A., Allen, A.P., Ingleton, T., Armand, L., 2014. A decadal decline in relative
805 abundance and a shift in microphytoplankton composition at a long-term coastal station
806 off southeast Australia. Limnol. Oceanogr. 59, 519–531. doi:10.4319/lo.2014.59.2.0519

807 Andrew, A.A., Del Vecchio, R., Subramaniam, A., Blough, N. V., 2013. Chromophoric
808 dissolved organic matter (CDOM) in the Equatorial Atlantic Ocean: Optical properties
809 and their relation to CDOM structure and source. Mar. Chem. 148, 33–43.
810 doi:10.1016/j.marchem.2012.11.001

811 Aurin, D. a, Dierssen, H.M., 2012. Advantages and limitations of ocean color remote sensing
812 in CDOM-dominated , mineral-rich coastal and estuarine waters. Remote Sens. Environ.
813 125, 181–197. doi:10.1016/j.rse.2012.07.001

814 Babin, M., Stramski, D., Ferrari, G.M., Claustre, H., Bricaud, A., Obolensky, G., Hoepffner,

N., 2003. Variations in the light absorption coefficients of phytoplankton, nonalgal particles, and dissolved organic matter in coastal waters around Europe. J. Geophys. Res. 108, 3211. doi:10.1029/2001JC000882

Barker, K., Smyth, T., Lavender, S., Aiken, J., 2007. A novel technique to estimate primary production directly from earth observation data: An inherent optical property approach, in: Envisat Symposium 2007. Montreux, Switzerland.

Barlow, R.G., Aiken, J., Moore, G.F., Holligan, P.M., Lavender, S., 2004. Pigment adaptations in surface phytoplankton along the eastern boundary of the Atlantic Ocean. Mar. Ecol. Prog. Ser. 281, 13–26. doi:10.3354/meps281013

Barnes, M.K., Tilstone, G.H., Smyth, T.J., Suggett, D.J., Astoreca, R., Lancelot, C., Kromkamp, J.C., 2014. Absorption-based algorithm of primary production for total and size-fractionated phytoplankton in coastal waters. Mar. Ecol. Prog. Ser. 504, 73–89. doi:10.3354/meps10751

Behrenfeld, M.J., Falkowski, P.G., 1997. Photosynthetic rates derived from satellite-based chlorophyll concentration. Limnol. Oceanogr. 42, 1–20.

Behrenfeld, M.J., O'Malley, R.T., Boss, E.S., Westberry, T.K., Graff, J.R., Halsey, K.H., Milligan, A.J., Siegel, D. a., Brown, M.B., 2016. Revaluating ocean warming impacts on global phytoplankton. Nat. Clim. Chang. 323–330. doi:10.1038/nclimate2838

Bender, M., Orchardo, J., Dickson, M., Barber, R., Lindley, S., 1999. In vitro O 2 fluxes compared with 14 C production and other rate terms during the JGOFS Equatorial Pacific experiment. Deep Sea Res. Part I Oceanogr. Res. Pap. 46, 637–654.

Blondeau-Patissier, D., Brando, V.E., Oubelkheir, K., Dekker, a. G., Clementson, L. a., Daniel, P., 2009. Bio-optical variability of the absorption and scattering properties of the Queensland inshore and reef waters, Australia. J. Geophys. Res. Ocean. 114, C05003. doi:10.1029/2008JC005039

Blondeau-Patissier, D., Dekker, A., Schroeder, T., Brando, V., 2011. Phytoplankton dynamics in shelf waters around Australia, Australia State of the Environment 2011. Canberra.

Bouman, H.A., Nakane, T., Oka, K., Nakata, K., Kurita, K., Sathyendranath, S., Platt, T., 2010. Environmental controls on phytoplankton production in coastal ecosystems : A case study from Tokyo Bay. Estuar. Coast. Shelf Sci. 87, 63–72. doi:10.1016/j.ecss.2009.12.014

Bouman, H. a., Platt, T., Kraay, G.W., Sathyendranath, S., Irwin, B.D., 2000. Bio-optical properties of the subtropical North Atlantic. I. Vertical variability. Mar. Ecol. Prog. Ser. 200, 3–18. doi:10.3354/meps200003

Brando, V.E., Dekker, A.G., Park, Y.J., Schroeder, T., 2012. Adaptive semianalytical inversion of ocean color radiometry in optically complex waters. Appl. Opt. 51, 2808–2833. doi:10.1364/AO.51.002808

Brewin, R.J.W., Sathyendranath, S., Hirata, T., Lavender, S.J., Barciela, R.M., Hardman-Mountford, N.J., 2010. A three-component model of phytoplankton size class for the Atlantic Ocean. Ecol. Modell. 221, 1472–1483. doi:10.1016/j.ecolmodel.2010.02.014

Bricaud, A., Claustre, H., Ras, J., Oubelkheir, K., 2004. Natural variability of

857 phytoplanktonic absorption in oceanic waters: Influence of the size structure of algal
858 populations. J. Geophys. Res. Ocean. 109, 1–12. doi:10.1029/2004JC002419

859 Brunet, C., Lizon, F., 2003. Tidal and diel periodicities of size-fractionated phytoplankton
860 pigment signatures at an offshore station in the southeastern English Channel. Estuar.
861 Coast. Shelf Sci. 56, 833–843. doi:10.1016/S0272-7714(02)00323-2

862 Burford, M.A., Rothlisberg, P.C., Revill, A.T., 2009. Sources of nutrients driving production
863 in the Gulf of Carpentaria, Australia: a shallow tropical shelf system. Mar. Freshw. Res.
864 60, 1044–1053.

865 Burford, M. a., Revill, a. T., Palmer, D.W., Clementson, L., Robson, B.J., Webster, I.T.,
866 2011. River regulation alters drivers of primary productivity along a tropical river-
867 estuary system. Mar. Freshw. Res. 62, 141–151. doi:10.1071/MF10224

868 Campbell, J.W., 1995. The lognormal distribution as a model for bio-optical variability in the
869 sea. J. Geophys. Res. Atmos. 100, 13237–13254. doi:10.1029/95JC00458

870 Cermeño, P., Estévez-Blanco, P., Marañón, E., Fernández, E., 2005. Maximum
871 photosynthetic efficiency of size-fractionated phytoplankton assessed by 14C uptake and
872 fast repetition rate fluorometry. Limnol. Oceanogr. 50, 1438–1446.
873 doi:10.4319/lo.2005.50.5.1438

874 Chavez, F.P., Messié, M., Pennington, J.T., 2011. Marine primary production in relation to
875 climate variability and change. Ann. Rev. Mar. Sci. 3, 227–260.
876 doi:10.1146/annurev.marine.010908.163917

877 Cherukuru, N., Brando, V.E., Schroeder, T., Clementson, L. a., Dekker, A.G., 2014.
878 Influence of river discharge and ocean currents on coastal optical properties. Cont. Shelf
879 Res. 84, 188–203. doi:10.1016/j.csr.2014.04.022

880 Cherukuru, N., Davies, P.L., Brando, V.E., Anstee, J.M., Baird, M.E., Clementson, L.A.,
881 Doblin, M.A., 2016. Physical oceanographic processes influence bio-optical properties
882 in the Tasman Sea. J. Sea Res. 110, 1–7. doi:10.1016/j.seares.2016.01.008

883 Clarke, K.R., Warwick, R.M., 2001. Change in Marine Communities: An approach to
884 statistical analysis and interpretation, 2nd ed. PRIMER-E Ltd, Plymouth.

885 Clementson, L.A., Parslow, J.S., Turnbull, A.R., Bonham, P.I., 2004. Properties of light
886 absorption in highly coloured estuarine system in south-east Australia which is prone to
887 blooms of the toxic dinoflgellate Gymnodinium catenatum. Estuar. Coast. Shelf Sci. 60,
888 101–112. doi:10.1016/j.ecss.2003.11.022

889 Cloern, J.E., Foster, S.Q., Kleckner, a. E., 2014. Phytoplankton primary production in the
890 world's estuarine-coastal ecosystems. Biogeosciences 11, 2477–2501. doi:10.5194/bg-
891 11-2477-2014

892 Condie, S. a., Dunn, J.R., 2006. Seasonal characteristics of the surface mixed layer in the
893 Australasian region: Implications for primary production regimes and biogeography.
894 Mar. Freshw. Res. 57, 569–590. doi:10.1071/MF06009

895 Cowley, R., Critchley, G., Eriksen, R., Latham, V., Plaschke, R., Rayner, M., Terhell, D.,
896 1999. CSIRO Marine Laboratories Report 236 Hydrochemistry Operations Manual.
897 Hobart.

898 Dakin, W.J., Colefax, A., 1940. The plankton of the Australian coastal waters of New South

899 Wales. Part 1. Dep. Zool. Monogr. 1, 303–314.

900 Dakin, W.J., Colefax, A., 1933. The marine plankton of the coastal waters of New South
901 Wales. 1. The chief planktonic forms and their seasonal distribution. Proc. Linn. Soc.
902 New South Wales 58, 186–222.

903 de Boyer Montégut, C., Madec, G., Fischer, A.S., Lazar, A., Iudicone, D., 2004. Mixed layer
904 depth over the global ocean: An examination of profile data and a profile-based
905 climatology. J. Geophys. Res. C Ocean. 109, 1–20. doi:10.1029/2004JC002378

906 Del Vecchio, R., Blough, N., 2002. Photobleaching of chromophoric dissolved organic matter
907 in natural waters: kinetics and modeling. Mar. Chem. 78, 231–253. doi:10.1016/S0304-
908 4203(02)00036-1

909 Devlin, M.J., Brodie, J., 2005. Terrestrial discharge into the Great Barrier Reef Lagoon:
910 Nutrient behavior in coastal waters. Mar. Pollut. Bull. 51, 9–22.
911 doi:10.1016/j.marpolbul.2004.10.037

912 Devred, E., Sathyendranath, S., Stuart, V., Platt, T., 2011. A three component classification
913 of phytoplankton absorption spectra: Application to ocean-color data. Remote Sens.
914 Environ. 115, 2255–2266. doi:10.1016/j.rse.2011.04.025

915 Everett, J.D., Baird, M.E., Roughan, M., Suthers, I.M., Doblin, M.A., 2014. Relative impact
916 of seasonal and oceanographic drivers on surface chlorophyll a along a Western
917 Boundary Current. Prog. Oceanogr. 120, 340–351. doi:10.1016/j.pocean.2013.10.016

918 Everett, J.D., Doblin, M.A., 2015. Characterising primary productivity measurements across
919 a dynamic western boundary current region. Deep Sea Res. Part I Oceanogr. Res. Pap.
920 100, 105–116. doi:10.1016/j.dsr.2015.02.010

921 Finkel, Z.V., 2001. Light absorption and size scaling of light-limited metabolism in marine
922 diatoms. Limnol. Oceanogr. 46, 86–94. doi:10.4319/lo.2001.46.1.0086

923 Finkel, Z. V., 2014. Marine Net Primary Production, in: Freedman, B. (Ed.), Global
924 Environmental Change. Springer Science + Business Media, Dordrecht, pp. 292–305.
925 doi:10.1016/j.gloenvcha.2008.10.009

926 Foukal, N.P., Thomas, A.C., 2014. Biogeography and phenology of satellite-measured
927 phytoplankton seasonality in the California current. Deep. Res. Part I 92, 11–25.
928 doi:10.1016/j.dsr.2014.06.008

929 Frouin, R.J., Kampel, M., 2014. Estimating solar radiation absorbed by live phytoplankton
930 from satellite ocean-color data Estimating Solar Radiation Absorbed by Live
931 Phytoplankton from Satellite Ocean-Color Data, in: Frouin, R.J., Pan, D., Murakami, H.
932 (Eds.), Proceedings of the Interational Society for Optics and Photonics: Ocean Remote
933 Sensing and Monitoring from Space. pp. 0–10. doi:10.1117/12.2074004

934 Furnas, M.J., 2003. Catchments and Corals: Terrestrial runoff to the Great Barrier Reef.
935 CRC/AIMS, Townsville.

936 Furnas, M.J., Carpenter, E.J., 2016. Primary production in the tropical continental shelf seas
937 bordering northern Australia. Cont. Shelf Res. 129, 33–48.
938 doi:10.1016/j.csr.2016.06.006

939 Furnas, M.J., Mitchell, A.W., 1987. Phytoplankton dynamics in the central Great Barrier
940 Reef II. Primary production. Cont. Shelf Res. 7, 1049–1062. doi:doi:10.1016/0278-

941 4343(87)90098-7

942 Gazeau, F., Smith, S.V., B., G., Frankignoulle, M., J-P., G., 2004. The European coastal
943 zone: characterization and first assessment of ecosystem metabolism. Estuar. Coast.
944 Shelf Sci. 60, 673–694.

945 Giannini, M.F.C., Ciotti, Á.M., 2016. Parameterization of natural phytoplankton photo-
946 physiology: Effects of cell size and nutrient concentration. Limnol. Oceanogr.
947 doi:10.1002/lno.10317

948 Glibert, P.M., Heil, C.A., O'Neil, J.M., Dennison, W.C., O'Donohue, M.J.H., 2006. Nitrogen
949 , Phosphorus , Silica , and Carbon in Moreton Bay , Queensland , Australia : Differential
950 Limitation of Phytoplankton Biomass and Production. Estuaries and Coasts 29, 209–
951 221.

952 Grande, K.D., Williams, B., Marra, J.F., Purdie, A., Heinemann, K., Eppley, R.W., Bender,
953 M.L., 1989. Primary production in the North Pacific Central Gyre: A comparison of
954 rates determined by the 14C, O2 concentration and 18O methods. Deep Sea Res. Part A.
955 Oceanogr. Res. Pap. 36, 1621–1634.

956 Green, S. a., Blough, N. V., 1994. Optical absorption and fluorescence properties of
957 chromophoric dissolved organic matter in natural waters. Limnol. Oceanogr. 39, 1903–
958 1916. doi:10.4319/lo.1994.39.8.1903

959 Hama, T., Miyazaki, T., Ogawa, Y., Iwakuma, T., Takahashi, M., Otsuki, A., Ichimura, S.,
960 1983. Measurement of photosynthetic production of a marine phytoplankton population
961 using a stable 13C isotope. Mar. Biol. 73, 31–36.

962 Hanson, C.E., Pattiaratchi, C.B., Waite, A.M., 2005. Seasonal production regimes off south-
963 western Australia: Influence of the Capes and Leeuwin Currents on phytoplankton
964 dynamics. Mar. Freshw. Res. 56, 1011–1026. doi:10.1071/MF04288

965 Hanson, C.E., Pesant, S., Waite, A.M., Pattiaratchi, C.B., 2007. Assessing the magnitude and
966 significance of deep chlorophyll maxima of the coastal eastern Indian Ocean. Deep. Res.
967 Part II Top. Stud. Oceanogr. 54, 884–901. doi:10.1016/j.dsr2.2006.08.021

968 Hassler, C.S., Djajadikarta, J.R., Doblin, M. a., Everett, J.D., Thompson, P. a., 2011.
969 Characterisation of water masses and phytoplankton nutrient limitation in the East
970 Australian Current separation zone during spring 2008. Deep. Res. Part II Top. Stud.
971 Oceanogr. 58, 664–677. doi:10.1016/j.dsr2.2010.06.008

972 Hayes, D., Lyne, V., Condie, S., Griffits, B., Pigot, S., Hallegraeff, G., 2005. Collation and
973 analysis of oceanographic datasets for national marine bioregionalisation.

974 Hirata, T., Aiken, J., Hardman-Mountford, N., Smyth, T.J., Barlow, R.G., 2008. An
975 absorption model to determine phytoplankton size classes from satellite ocean colour.
976 Remote Sens. Environ. 112, 3153–3159. doi:10.1016/j.rse.2008.03.011

977 Hirata, T., Hardman-Mountford, N.J., Barlow, R., Lamont, T., Brewin, R., Smyth, T., Aiken,
978 J., 2009. An inherent optical property approach to the estimation of size-specific
979 photosynthetic rates in eastern boundary upwelling zones from satellite ocean colour:
980 An initial assessment. Prog. Oceanogr. 83, 393–397. doi:10.1016/j.pocean.2009.07.019

981 Hirawake, T., Takao, S., Horimoto, N., Ishimaru, T., Yamaguchi, Y., Fukuchi, M., 2011. A
982 phytoplankton absorption-based primary productivity model for remote sensing in the

983 Southern Ocean. Polar Biol. 34, 291–302. doi:10.1007/s00300-010-0949-y

984 Johnson, J., Jeffrey, M., Devlin, M., Wilkinson, S., Anthony, K., Yorkston, H., Heron, S.,
985 Puotinen, M., van Hooidonk, R., 2013. 2013 Scientific Consensus Statement: Resilience
986 of Great Barrier Reef ecosystems and drivers of change.

987 Jones, E.M., Doblin, M.A., Matear, R., King, E., 2015. Assessing and evaluting the ocean-
988 colour footprint of a regional observing system. J. Mar. Syst. 143, 49–61.
989 doi:10.1016/j.jmarsys.2014.10.012

990 Kelly, P., Clementson, L., Lyne, V., 2015. Decadal and seasonal changes in temperature,
991 salinity, nitrate, and chlorophyll in inshore and offshore waters along southeast
992 Australia. J. Geophys. Res. Ocean. 1–19. doi:10.1002/2014JC010646

993 Kiefer, D.A., Mitchell, B.G., 1983. A simple steady state description of phytoplankton
994 growth based on absorption cross section and quantum efficiency. Limnol. Oceanogr.
995 28, 770–776. doi:10.4319/lo.1983.28.4.0770

996 Kirk, J.T.O., 2011. Light and Photosynthesis in Aquatic Ecosystems, 3rd ed. Cambridge
997 University Press.

998 Knap, A.H., Michaels, A., Close, A.R., Ducklow, H., Dickson, A.G., 1996. Protocols for the
999 Joint Global Ocean Flux Study (JGOFS) Core Measurements. Reprint of the IOC
1000 Manuals and Guides No. 29. doi:10013/epic.27912

1001 Langdon, C., 1993. The significance of respiration in production measurements based on
1002 oxygen. ICES Mar. Sci. Symp. 197, 69–78.

1003 Lavaud, J., Strzepek, R.F., Kroth, P.G., 2007. Photoprotection capacity differs among
1004 diatoms: Possible consequences on the spatial distribution of diatoms related to
1005 fluctuations in the underwater light climate. Limnol. Oceanogr. 52, 1188–1194.
1006 doi:10.4319/lo.2007.52.3.1188

1007 Lee, Z., Marra, J., Perry, M.J., Kahru, M., 2015. Estimating oceanic primary productivity
1008 from ocean color remote sensing: A strategic assessment. J. Mar. Syst. 149, 50–59.
1009 doi:10.1016/j.jmarsys.2014.11.015

1010 Lee, Z.P., Carder, K.L., Marra, J., Steward, R.G., Perry, M.J., 1996. Estimating primary
1011 production at depth from remote sensing. Appl. Opt. 35, 463–474.
1012 doi:10.1364/AO.35.000463

1013 Lewis, M., Smith, J., 1983. A small volume, short-incubation-time method for measurement
1014 of photosynthesis as a function of incident irradiance. Mar. Ecol. Prog. Ser. 13, 99–102.
1015 doi:10.3354/meps013099

1016 Limpert, E., Stahel, W.A., Abbt, M., 2001. Log-normal Distributions across the Sciences :
1017 Keys and Clues. Bioscience 51, 341–352.

1018 Lynch, T.P., Morello, E.B., Evans, K., Richardson, A.J., Rochester, W., Steinberg, C.R.,
1019 Roughan, M., Thompson, P., Middleton, J.F., Feng, M., Sherrington, R., Brando, V.,
1020 Tilbrook, B., Ridgway, K., Allen, S., Doherty, P., Hill, K., Moltmann, T.C., 2014. IMOS
1021 National Reference Stations : A Continental-Wide Physical , Chemical and Biological
1022 Coastal Observing System. PLoS One 9, 1–28. doi:10.1371/journal.pone.0113652

1023 Ma, S., Tao, Z., Yang, X., Yu, Y., Zhou, X., Ma, W., Li, Z., 2014. Estimation of marine
1024 primary productivity from satellite-derived phytoplankton absorption data. IEEE J. Sel.

1025 Top. Appl. Earth Obs. Remote Sens. 7, 3084–3092. doi:10.1109/JSTARS.2014.2298863

1026 Marra, J., 2009. Net and gross productivity: Weighing in with 14C. Aquat. Microb. Ecol. 56,
1027 123–131. doi:10.3354/ame01306

1028 Marra, J., 2002. Approaches to the measurement of plankton production, in: Williams, P.J.,
1029 Tomas, D.N., Reynolds, C.S. (Eds.), Phytoplankton Productivity: Carbon Assimilation
1030 in Marine and Freshwater Ecosystems. Blackwell Science Inc, Oxford, pp. 78–108.

1031 Marra, J., Barber, R.T., 2004. Phytoplankton and heterotrophic respiration in the surface layer
1032 of the ocean. Geophys. Res. Lett. 31, 12–15. doi:10.1029/2004GL019664

1033 Marra, J., Ho, C., Trees, C.C., 2003. An Alternative Algorithm for the Calculation of Primary
1034 Productivity from Remote Sensing Data, LDEO Technical Report. New York City.

1035 Marra, J., Trees, C.C., O'Reilly, J.E., 2007. Phytoplankton pigment absorption: A strong
1036 predictor of primary productivity in the surface ocean. Deep. Res. Part I Oceanogr. Res.
1037 Pap. 54, 155–163. doi:10.1016/j.dsr.2006.12.001

1038 Marra, J.F., Lee, Z., Halloran, C., 2016. A databse for in situ primary production based on
1039 Carbon-14 assimilation, in: Ocean Optics XXIII Conference. p. 1.

1040 Mélin, F., Vantrepotte, V., 2015. How optically diverse is the coastal ocean? Remote Sens.
1041 Environ. 160, 235–251. doi:10.1016/j.rse.2015.01.023

1042 Mitchell, B.G., Kahru, M., Wieland, J., Stramska, M., 2002. Determination of spectral
1043 absorption coefficients of particles, dissolved material and phytoplankton for discrete
1044 water samples., in: Mueller, J.L., Fargion, G.S., McClain, C.R., Pegau, S., Ronald, J.,
1045 Zaneveld, V., Mitchell, B.G., Kahru, M., Wieland, J., Stramska, M. (Eds.), Ocean Optics
1046 Protocols for Satellite Ocean Color Sensor Validation, Revision 4, Volume IV: Inherent
1047 Optical Properties: Instruments, Characterizations, Field Measurements and Data
1048 Analysis Protocols. National Aeronautical and Space Administration, Maryland, pp.
1049 231–57.

1050 Moore, T.S., Campbell, J.W., Dowell, M.D., 2009. A class-based approach to characterizing
1051 and mapping the uncertainty of the MODIS ocean chlorophyll product. Remote Sens.
1052 Environ. 113, 2424–2430. doi:10.1016/j.rse.2009.07.016

1053 Morel, A., 1991. Light and marine photosynthesis: a spectral model with geochemical and
1054 climatological implications. Prog. Oceanogr. 26, 263–306.

1055 Mousseau, L., Dauchez, S., Legendre, L., Fortier, L., 1995. Photosynthetic carbon uptake by
1056 marine phytoplankton: comparison of the stable (13C) and radioactive (14C) isotope
1057 methods. J. Plankton Res. 17, 1449–1460. doi:10.1093/plankt/17.7.1449

1058 Odermatt, D., Gitelson, A., Brando, V.E., Schaepman, M., 2012. Review of constituent
1059 retrieval in optically deep and complex waters from satellite imagery. Remote Sens.
1060 Environ. 118, 116–126. doi:10.1016/j.rse.2011.11.013

1061 Oliver, M.J., Schofield, O., Bergmann, T., Glenn, S., Orrico, C., Moline, M., 2004. Deriving
1062 in situ phytoplankton absorption for bio-optical productivity models in turbid waters. J.
1063 Geophys. Res. C Ocean. 109, 1–12. doi:10.1029/2002JC001627

1064 Oubelkheir, K., Clementson, L. a., Webster, I.T., Ford, P.W., Dekker, A.G., Radke, L.C.,
1065 Daniel, P., 2006. Using inherent optical properties to investigate biogeochemical
1066 dynamics in a tropical macrotidal coastal system. J. Geophys. Res. Ocean. 111, 1–15.

1067 doi:10.1029/2005JC003113

1068 Oubelkheir, K., Ford, P.W., Clementson, L.A., Cherukuru, N., Fry, G., Steven, A.D.L., 2014.
1069 Impact of an extreme flood event on optical and biogeochemical properties in a
1070 subtropical coastal periurban embayment (Eastern Australia). J. Geophys. Res. Ocean.
1071 119, 6024–6045. doi:10.1002/2014JC010205

1072 Patt, F.S., Barnes, R.A., Eplee, R.E., Franz, B.A., Robinson, W.D., Feldman, G.C., Bailey,
1073 S.W., Gales, J., Werdell, P.J., Wang, M., Frouin, R., Stumpf, R.P., Arnone, R.A., Gould,
1074 R.W., Martinolich, P.M., O'Reilly, J.E., Yoder, J.A., 2003. Algorithm Updates for the
1075 Fourth SeaWiFS Data Reprocessing, NASA Technical Memorandum 2003–206892.

1076 Pauly, D., Christensen, V., 1995. Primary production required to sustain global fisheries.
1077 Nature 374, 255–257. doi:10.1038/374255a0

1078 Platt, T., Gallegos, C.L., Harrison, W.G., 1980. Photoinibition of photosynthesis in natural
1079 assemblages of marine phytoplankton. J. Mar. Res. 38, 687–701. doi:citeulike-article-
1080 id:3354339

1081 Qin, Y., Brando, V.E., Dekker, A.G., Blondeau-Patissier, D., 2007. Validity of SeaDAS
1082 water constituents retrieval algorithms in Australian tropical coastal waters. Geophys.
1083 Res. Lett. 34, 1–4. doi:10.1029/2007GL030599

1084 Regaudie-de-gioux, A., Lasternas, S., Agustí, S., Duarte, C.M., 2014. Comparing marine
1085 primary production estimates through different methods and development of conversion
1086 equations. Front. Mar. Sci. Mar. Biogeochem. 1, 1–14. doi:10.3389/fmars.2014.00019

1087 Robinson, C., Suggett, D.J., Cherukuru, N., Ralph, P.J., Doblin, M.A., 2014. Performance of
1088 Fast Repetition Rate fluorometry based estimates of primary productivity in coastal
1089 waters. J. Mar. Syst. 139, 299–310. doi:10.1016/j.jmarsys.2014.07.016

1090 Robinson, C., Tilstone, G., Rees, A., Smyth, T., Fishwick, J., Tarran, G., Luz, B., Barkan, E.,
1091 David, E., 2009. Comparison of in vitro and in situ plankton production determinations.
1092 Aquat. Microb. Ecol. 54, 13–34. doi:10.3354/ame01250

1093 Roughan, M., Middleton, J.H., 2002. A comparison of observed upwelling mechanisms off
1094 the east coast of Australia. Cont. Shelf Res. 22, 2551–2572. doi:10.1016/S0278-
1095 4343(02)00101-2

1096 Sathyendranath, S., Stuart, V., Nair, A., Oka, K., Nakane, T., Bouman, H., Forget, M.H.,
1097 Maass, H., Platt, T., 2009. Carbon-to-chlorophyll ratio and growth rate of phytoplankton
1098 in the sea. Mar. Ecol. Prog. Ser. 383, 73–84. doi:10.3354/meps07998

1099 Sauer, M.J., Roesler, C.S., Werdell, P.J., Barnard, A., 2012. Under the hood of satellite
1100 empirical chlorophyll a algorithms: revealing the dependencies of maximum band ratio
1101 algorithms on inherent optical properties. Opt. Express. doi:10.1364/OE.20.020920

1102 Shang, S.L., Behrenfeld, M.J., Lee, Z.P., Malley, R.T.O., Wei, G.M., Li, Y.H., Westberry, T.,
1103 2010. Comparison of primary productivity models in the Southern Ocean-preliminary
1104 results, in: Proc. SPIE 7678, Ocean Sensing and Monitoring II, 767808.

1105 Silsbe, G.M., Behrenfeld, M.J., Halsey, K.H., J, M.A., Westberry, T.K., 2016. The CAFE
1106 model: A net production model for global ocean phytoplankton. Glob. Biogeochem.
1107 Cycles 1–22. doi:10.1002/2016GB00552521

1108 Steeman Nielsen, E., Hansen, V.K., 1958. Measurements with the carbon-14 technique of the

1109 respiration rates in natural populations of phytoplankton. Deep Sea Res. 5, 222–233.
1110 doi:10.1016/0146-6313(58)90015-7

1111 Suggett, D.J., Moore, C.M., Maranon, E., Omachi, C., Varela, R.A., Aiken, J., Holligan,
1112 P.M., 2006. Photosynthetic electron turnover in the tropical and subtropical Atlantic
1113 Ocean. Deep. Res. Part II Top. Stud. Oceanogr. 53, 1573–1592.
1114 doi:10.1016/j.dsr2.2006.05.014

1115 Tassan, S., Ferrari, G.M., 1995. An alternative approach to absorption measurements of
1116 aquatic particles retained on filters. Limnol. Oceanogr. 40, 1358–1368.
1117 doi:10.4319/lo.1995.40.8.1358

1118 Thompson, P.A., Baird, M.E., Ingleton, T., Doblin, M.A., 2009. Long-term changes in
1119 temperate Australian coastal waters: Implications for phytoplankton. Mar. Ecol. Ser.
1120 394, 1–19. doi:10.3354/meps08297

1121 Tilstone, G.H., Angel-Benavides, I.M., Pradhan, Y., Shutler, J.D., Groom, S.,
1122 Sathyendranath, S., 2011. An assessment of chlorophyll-a algorithms available for
1123 SeaWiFS in coastal and open areas of the Bay of Bengal and Arabian Sea. Remote Sens.
1124 Environ. 115, 2277–2291. doi:10.1016/j.rse.2011.04.028

1125 Uitz, J., Claustre, H., Morel, A., Hooker, S.B., 2006. Vertical distribution of phytoplankton
1126 communities in open ocean: An assessment based on surface chlorophyll. J. Geophys.
1127 Res. 111, C08005. doi:10.1029/2005jc003207

1128 Uitz, J., Huot, Y., Bruyant, F., Babin, M., Claustre, H., 2008. Relating phytoplankton
1129 photophysiological properties to community structure on large scales. Limnol.
1130 Oceanogr. 53, 614–630. doi:10.4319/lo.2008.53.2.0614

1131 Van Heukelem, L., Thomas, C.S., 2001. Computer-assisted high-performance liquid
1132 chromatography method development with applications to the isolation and analysis of
1133 phytoplankton pigments. J. Chromatogr. A 910, 31–49.

1134 van Ruth, P.D., Ganf, G.G., Ward, T.M., 2010. The influence of mixing on primary
1135 productivity: A unique application of classical critical depth theory. Prog. Oceanogr. 85,
1136 224–235. doi:10.1016/j.pocean.2010.03.002

1137 Vidussi, F., Claustre, H., Manca, B.B., Luchetta, A., Marty, J.-C., 2001. Phytoplankton
1138 pigment distribution in relation to upper Francesca Claustre For the whole Tchl a
1139 concentration mg estimated production value being mg m and the highest
1140 picophytoplankton contribution of Tchl a •. gyres by low Tchl a concentrations and. J.
1141 Geophys. Res. 106, 939–956.

1142 Wang, M., Tang, J., Shi, W., 2007. MODIS-derived ocean color products along the China
1143 east coastal region 34, 1–5. doi:10.1029/2006GL028599

1144 Werdell, P.J., Franz, B. a, Bailey, S.W., Feldman, G.C., Boss, E., Brando, V.E., Dowell, M.,
1145 Hirata, T., Lavender, S.J., Lee, Z., Loisel, H., Maritorena, S., Mélin, F., Moore, T.S.,
1146 Smyth, T.J., Antoine, D., Devred, E., D'Andon, O.H.F., Mangin, A., 2013. Generalized
1147 ocean color inversion model for retrieving marine inherent optical properties. Appl. Opt.
1148 52, 2019–37. doi:10.1364/AO.52.002019

1149 Westberry, T.K., Behrenfeld, M.J., 2014. Oceanic Net Primary Production, in: Hanes, J.M.
1150 (Ed.), Biophysical Applications of Satellite Remote Sensing. Springer Remote
1151 Sensing/Photogrammery, Heidelberg, pp. 205–228. doi:10.1007/978-3-642-25047-7

1152 Wollast, R., 1998. Evaluation and comparison of the global carbon cycle in the coastal zone
1153 and in the open ocean., in: Brin, K.H., Robinson, A.R. (Eds.), The Sea: The Global
1154 Coastal Ocean, Processes and Methods. John Wiley & Sons, New York, pp. 213–252.

1155 Yoder, J. a., Schollaert, S.E., O'Reilly, J.E., 2002. Climatological phytoplankton chlorophyll
1156 and sea surface temperature patterns in continental shelf and slope waters off the
1157 northeast U.S. coast. Limnol. Oceanogr. 47, 672–682. doi:10.4319/lo.2002.47.3.0672

1158

**Tables**

Table 1. Locations of sampling stations and variability in physical conditions, dissolved nutrients and phytoplankton chlorophyll-*a* concentration and net primary productivity (mean(±standard deviation)).

| Voyage/Mooring | V1 SS2010_v03 | V2 SS2010_v09 | V3 SS2013_t03 | V4 eReefs_2013 | Port Hacking |
|---|---|---|---|---|---|
| **Region** | North-west | Eastern Australia | Northern Australia | Great Barrier Reef | South-eastern |
| **Latitude** | 16.689 °S to | 28.878 °S to 32.364 | 9.775 °S to 19.901 | 13.946 °S to 18.083 | 34.116 °S to 34.137 |
| **Longitude** | 123.346 °E to | 152.688 °E to | 122.007 °E to | 144.202 °E to | 151.206 °E to |
| **Season** | Autumn | Spring | Winter | Summer | Monthly |
| **No. stations** | 5 | 14 | 10 | 4 | 8 |
| **NPP Method** | $^{14}$C 1 h* | $^{14}$C 24 h$^{\#}$ | $^{13}$C 24 h$^{\wedge}$ | $^{13}$C 4-24 h$^{\#}$ | $^{14}$C 24 h$^{\#}$ |
| **Temperature (°C)** | 31.3(±0.15) | 21.2(±0.72) | 25.5(±1.16) | 28.9(±1.45) | 20.1(±1.93) |
| **Salinity** | 35.4(±0.15) | 35.4(±0.19) | 34.5(±0.71) | 33.0(±2.52) | 34.4(±0.15) |
| **$NO_3$** | 0.59(±0.61) | 0.59(±1.11) | 0.23(±0.37) | N.D. | 0.67(±0.77) |
| **$PO_4$** | 0.22(±0.02) | 0.14(±0.12) | 0.15(±0.07) | N.D. | 0.16(±0.09) |
| **Si** | 4.35(±0.92) | 0.76(±0.69) | 2.82(±1.91) | N.D. | 0.59(±0.30) |
| **$NH_4^+$** | 0.04(±0.03) | 0.20(±0.28) | 0.03(±0.08) | N.D. | 0.36(±0.31) |
| **TChl-*a* (mg m$^{-3}$)** | 0.95(±0.31) | 0.72(±1.04) | 0.43(±0.29) | 1.62(±0.97) | 0.72(±0.43) |
| **NPP (mmol C m$^{-3}$ d$^{-1}$)** | 4.01(±2.02) | 3.61(±6.23) | 2.14(±1.32) | 6.01(±3.58) | 3.85(±3.57) |
| **(min-max)** | (1.78-5.72) | (0.41-19.3) | (0.35-5.18) | (2.04-8.95) | (0.25-10.6) |

Symbols denote method used to estimate NPP: *small bottle method Lewis & Smith 1983; #JGOFs method for estimating NPP; ^method following Hama et al. 1983 and Burford et al. 2011 for estimating GPP and NPP.

1165 Table 2. Range (mean ± standard deviation) of optical component IOPs, NPP and chlorophyll-*a* concentration for each voyage.

| Region | V1<br>North-west Aust. | V2<br>Eastern Aust. | V3<br>Northern Aust. | V4<br>Great Barrier Reef | PHNRS<br>South-eastern |
|---|---|---|---|---|---|
| **$K_d$(PAR) ($m^{-1}$)** | 0.10-0.27<br>(0.16±0.07) | 0.04-0.25<br>(0.08±0.07) | 0.05-0.28<br>(0.14±0.07) | 0.15-0.47<br>(0.32±0.15) | 0.06-0.29<br>(0.14±0.08) |
| **$a_{TOT}$(440 nm) ($m^{-1}$)** | 0.097-0.371<br>(0.22±0.101) | 0.035-1.802<br>(0.299±0.455) | 0.013-1.261<br>(0.295±0.386) | 0.397-1.231<br>(0.845±0.306) | 0.045-0.433<br>(0.217-0.144) |
| **$a_{PHY}$(440 nm) ($m^{-1}$)** | 0.037-0.064<br>(0.055±0.011) | 0.011- 0.142<br>(0.038±0.040) | 0.008-0.042<br>(0.024±0.010) | 0.020-0.099<br>(0.0491±0.0315) | 0.013-0.048<br>(0.050±0.021) |
| **$a_{NAP}$(440 nm) ($m^{-1}$)** | 0.019-0.070<br>(0.039±0.026) | 0.002-0.586<br>(0.051±0.155) | 0.001-0.025<br>(0.011±0.009) | 0.013-0.262<br>(0.097±0.100) | 0.004-0.019<br>(0.011±0.006) |
| **$a_{CDOM}$(440 nm) ($m^{-1}$)** | 0.041-0.293<br>(0.139±0.100) | 0.021-1.122<br>(0.226±0.306) | 0.001-1.236<br>(0.026±0.387) | 0.300-0.942<br>0.699±0.249) | 0.004-0.416<br>(0.168±0.150) |
| **$a_{PHY}$(676 nm) ($m^{-1}$)** | 0.013-0.028<br>(0.022±0.006) | 0.003-0.069<br>(0.017±0.023) | 0.003-0.017<br>(0.009±0.005) | 0.007-0.049<br>(0.024±0.017) | 0.004-0.031<br>(0.015±0.010) |
| **$a_{PHY}$(PAR) ($m^{-1}$)** | 0.014-0.026<br>(0.023±0.005) | 0.004-0.073<br>(0.017±0.022) | 0.003-0.018<br>(0.009±0.005) | 0.050-0.009<br>(0.023±0.016) | 0.006-0.029<br>(0.016±0.008) |
| **$a_{PHY}$(440 nm)/$a_{PART}$(440 nm)** | 0.49-0.73<br>(0.62±0.12) | 0.14-0.93<br>(0.77±0.20) | 0.48-0.91<br>(0.76±0.16) | 0.24-0.83<br>(0.41±0.24) | 0.73-0.88<br>(0.79±0.05) |
| **$S_{NAP}$ ($nm^{-1}$)** | 0.010-0.012<br>(0.011±0.001) | 0.006-0.0152<br>(0.009±0.002) | 0.006-0.018<br>(0.012±0.005) | 0.009-0.018<br>(0.012±0.002) | 0.006-0.032<br>(0.020±0.010) |
| **$S_{CDOM}$ ($nm^{-1}$)** | 0.008-0.017<br>(0.012±0.004) | 0.001-0.019<br>(0.009±0.007) | 0.004-0.012<br>(0.008±0.003) | 0.006-0.016<br>(0.014±0.006) | 0.008-0.016<br>(0.013±0.003) |

Table 3.Model dependencies and output table.

| **Mathematical Model** | ***Equation* (coefficients(±S.E))** | ***n*** | $R^2$ | **RMSE** |
|---|---|---|---|---|
| NPP = $m \times a_{PHY}(PAR) + b$ | NPP = 304(±37.28) × $a_{PHY}(PAR)$ | 41 | 0.71 * | n.a. |
| Marra et al. 2007 | NPP = 510 × $a_{PHY}(PAR)$ + 0.0001 | | 0.84* | |
| NPP = $m \times a_{PHY}(440\ nm) + b$ | NPP = 123(±16.0) × $a_{PHY}(440\ nm)$ -1.03 | 41 | 0.65* | n.a. |
| NPP = $m \times a_{PHY}(676\ nm) + b$ | NPP = 297(±31.6) × $a_{PHY}(676\ nm)$-0.13 | 41 | 0.70* | n.a. |
| Absorption model 1: *NPP1*<br>NPP1 = $\bar{a}_{PHY} \times p \times 1000$ | NPP = 0.95(±0.10) × *NPP1* - 0.93 | 41 | 0.73* | 2.39 |
| Absorption model 2: *NPP2*<br>$NPP2 = \bar{E} \times \bar{a}_{PHY} \times \phi_m \times \phi_E \times 1000$ | NPP = 1.09(±0.12) × *NPP2* + 0.67 | 38 | 0.73* | 2.46 |
| Absorption model 3: *NPP3*<br>$NPP3 = \bar{a}_{PHY} \times p_s \times 1000$ | NPP = 0.78(±0.08) × *NPP3* + 0.17 | 41 | 0.72* | 2.44 |
| Absorption model 4: *NPP4*<br>$NPP3 = \bar{E} \times \bar{a}_{PHY} \times \phi \times 1000$ | NPP = 0.84(±0.12) × *NPP4* + 1.43 | 38 | 0.73* | 2.27 |

* = $p < 0.05$

1170

**Supplementary Tables**

Supplementary Table 1. Framework for predicting phytoplankton size class, biological response and environmental setting using the $\bar{a}_{PHY}$. Biological clusters were determined using multi-variate statistics outlined in section 2.6. Note that trends in $\bar{a}_{PHY}$ are also indicative of $a_{PHY}$(676 nm). Values in brackets are the average range (min-max) of parameters within each cluster. ^Aiken et al. (2008). #DistLM statistical tests, ↑ or ↓ indicates increasing or decreasing parameter values respectively.

| **Phytoplankton predictive framework using $a_{PHY}$ coefficient** | | | |
|---|---|---|---|
| Biological Cluster | 1 | 2 | 3 |
| **$\bar{a}_{PHY}$ ($m^{-1}$)** | High (0.02-0.08) | Medium (0.01-0.02) | Low (0.003-0.01) |
| **Aiken's bio-energetic status^** | High (Eutrophic) | Medium (Mesotrophic) | Low (Oligotrophic-Mesotrophic) |
| **NPP (mmol C $m^{-3}$ $d^{-1}$)** | High (12-30) | Low-Med (3-12) | Low (0-3) |
| **TChl-*a* (mg $m^{-3}$)** | High (1-2) | Medium (0.5 – 1) | Low (0.01-0.5) |
| **Dominant size class (%)** | Micro > 50 | Nano > 50 | Pico > 50 |
| **PPC/TP (ratio)** | Low (0.03-0.14) | Low-Med (0.03-0.16) | High (0.06-0.23) |
| **Quantum efficiency (mean±SEM)** | 0.030±0.009 | 0.015±0.008 | 0.008±0.006 |
| **Proportionality factor ($p_s$) (mean±SEM)** | 370±71 | 152±58 | 135±21 |
| **Light saturation*** | Light saturated | Light limited | Light saturated (extreme) |
| **Nutrient conditions*** | Replete | Replete | Deplete |
| ***Environmental parameters significantly correlated with#** | ↑ nitrate<br>↑ phosphate | ↑silicate<br>↑ $K_d$(PAR) | ↑ $E_Z$ (daily PAR)<br>↓$K_d$(PAR)<br>↓ MLD<br>↓Temp |

Supplementary Table 2. Marginal tests outlining the contribution of physical parameters to trends in biological parameters (NPP, TChl-*a*, $\bar{a}_{PHY}$, Φ, PPC/TP, microplankton, nanoplankton, picoplankton). Bold text indicates significance ($p < 0.05$).

| | Marginal tests | |
|---|---|---|
| **Predictor variable** | ***p*** | **Proportion** |
| T | 0.886 | 0.049 |
| MLD | 0.400 | 0.026 |
| *E* | 0.161 | 0.055 |
| $K_d$ | **0.000** | 0.337 |
| N | **0.001** | 0.217 |
| P | **0.000** | 0.418 |
| Si | **0.003** | 0.190 |
| $NH_4^+$ | 0.215 | 0.045 |

T=temperature, MLD=mixed layer depth, $E=\bar{E}$ daily irradiance, $K_d=K_d(PAR)$, N= nitrate, P=phosphate, Si=silicate, $NH_4^+$=ammonium

Supplementary Table 3. Overall best solutions for describing trends in the biological parameters (NPP, TChl-*a*, $\bar{a}_{PHY}$, Φ, PPC/TP, microplankton, nanoplankton, picoplankton) using physical parameters as predictors.

| | Best solutions | |
|---|---|---|
| **No. of variables** | **Selections** | $R^2$ |
| 1 | P | 0.43 |
| 2 | $K_d$, P, | 0.60 |
| 3 | $K_d$, P Si | 0.57 |
| 4 | $K_d$, N, P, Si | 0.59 |
| 5 | T, $K_d$, N, P, Si | 0.60 |
| 6 | T, $K_d$, *E*, N, P, Si | 0.62 |
| 7 | T, $K_d$, MLD, *E*, N, P, Si | 0.63 |
| All | T, $K_d$, MLD, *E*, N, P, Si, $NH_4^+$ | 0.65 |

T=temperature, MLD=mixed layer depth, $E=\bar{E}$ daily irradiance, $K_d=K_d$(PAR), N= nitrate, P=phosphate, Si=silicate, $NH_4^+$=ammonium

## Supplementary Figures

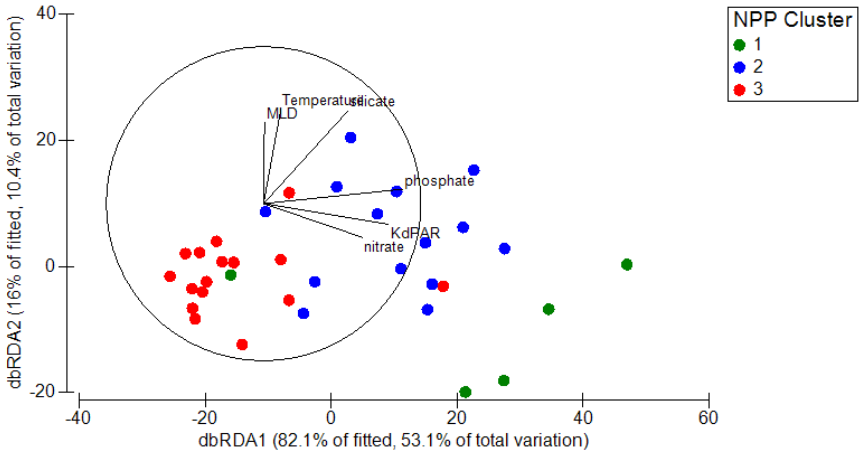


Supplementary Figure 1. Distance based linear models explaining the variability in NPP and $\bar{a}_{PHY}$ and other biological parameters, with environmental predictor parameters overlayed which best explained the variability. Numbers 1 – 3 and colours green, blue and red, respectively, indicate the biological clusters each sample belongs to, as outlined in section 3.4.

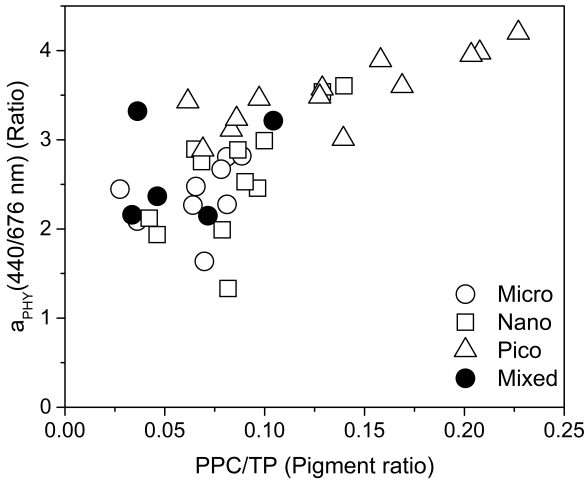


Supplementary Figure 2. The blue-to-red absorption ratio ($a_{PHY}$(440/676 nm)) as a function of the proportion of photoprotective pigments (PPC/TP). The blue-to-red ratio of the phytoplankton absorption coefficient ($a_{PHY}$(440/676 nm)) decreased with increasing TChl-*a* ($a_{PHY}$(440/676 nm) = 2.3921[TChl-*a*]$^{-0.192}$, $R^2$ = 0.64) and increased with the proportion of photoprotective pigments.

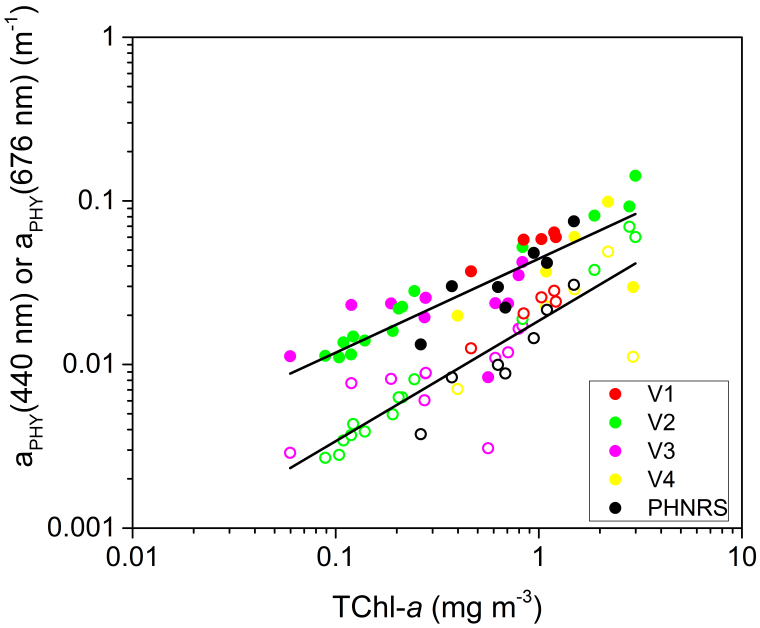


Supplementary Figure 3. Phytoplankton absorption coefficient at 440 nm (closed circles) and 676 nm (open circles) as a function of TChl-*a* concentration. Black line indicates fitted power function. The phytoplankton absorption coefficients at 440 nm and 676 nm both increased with TChl-*a* concentration according to a commonly accepted power function (Bricaud et al., 2004). The relationships between $a_{PHY}$ and TChl-*a* were both highly significant across all voyages and yielded the following functions: $a_{PHY}(440\ nm) = 0.0443[TChl\text{-}a]^{0.574}$ ($R^2 = 0.71$) and $a_{PHY}(676\ nm) = 0.0185[TChl\text{-}a]^{0.7387}$ ($R^2 = 0.80$). The relationship between $\bar{a}_{PHY}$ and TChl-*a* was very similar to $a_{PHY}(676\ nm)$ ($\bar{a}_{PHY} = 0.019[TChl\text{-}a]^{0.644}$, $R^2 = 0.76$) largely owing to the strong linear correlation between $\bar{a}_{PHY}$ and $a_{PHY}(676\ nm)$ ($R^2$=0.99).

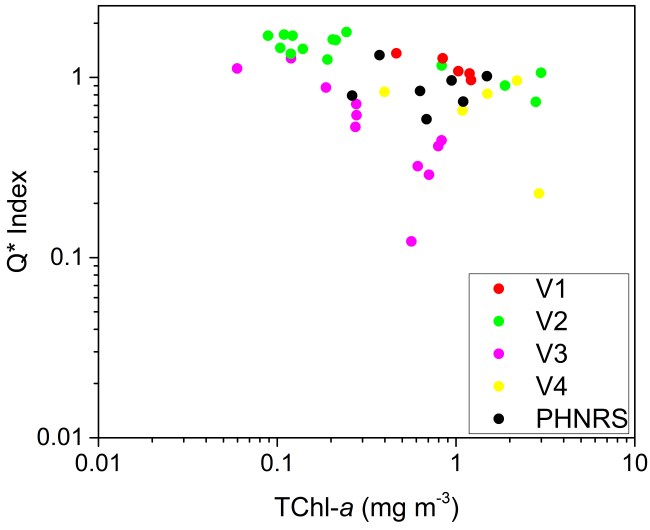


Supplementary Figure 4. Pigment packaging index (Q*) as a function of TChl-*a*. A reduction in Q* indicates increased pigment packaging (Bricaud et al., 2004; Morel and Bricaud, 1981). Variability in the $a_{PHY}$ parameter could also be explained by increased effects of pigment packaging (reduced Q* coefficient) in the phytoplankton cells with increasing TChl-*a*.

Samples from stations during V3 (northern Australian) appear to deviate from the general relationship, with even higher packaging impacts per unit chlorophyll-*a*.